[Monitoring of Coal Seam Gas Depressurisation using Geophysical Methods]

Thesis submitted in accordance with the requirements of the University of Adelaide for an Honours Degree in Geophysics

Joseph Rugari

November 2013

THE UNIVERSITY of ADELAIDE

MONITORING OF COAL SEAM GAS DEPRESSURISATION WITH GEOPHYSICS

GEOPHYSICAL MONITORING OF COAL SEAM GAS

ABSTRACT

Coal seam gas has emerged as a major industry in Australia over little more than a decade. Resource production inevitably relies on the extraction of groundwater from coal seams to depressurise coal measures, and allow natural gas flow. Current groundwater monitoring of a coal seam gas project uses expensive borehole sampling programs that can only provide point information, and improved monitoring of water extraction is suggested for existing and future wells.

This paper is a first stage feasibility study for surface magnetotelluric, and surface self-potential monitoring of a coal seam gas depressurisation event. The monitoring techniques used in this study directly measure fluid connectivity and dynamics to estimate the degree of porosity and permeability in a coal seam. In combination, the monitoring can provide both large scale and localised sub-surface fluid-flow modelling potential. The processes and its equipment are a practical, inexpensive and mobile solution for the expanding coal seam gas industry.

In this study synthetic modelling has been used with coal seam conditions, prototype self-potential monitoring equipment is constructed, and various monitoring equipment are tested in the field. Synthetic modelling has provided encouraging results, showing that a depressurisation event based in a Surat Basin Walloon Measures, southern Queensland, Australia geological model could be successfully monitored using magnetotelluric and self-potential methods. The prototype self-potential logger operated with a high level of precision, successfully mapping localised electrodes change of electric field at an aquifer pump test site; and the E-Logger instrument successfully recorded electric field data for magnetotelluric monitoring.

Overall, results present a great deal of potential for the combined effectiveness of magnetotelluric and self-potential monitoring methods in a coal seam gas depressurisation setting. Further studies, in particularly on-site depressurisation monitoring testing, is required to draw on more conclusive evidence.

KEYWORDS

Coal Seam Gas, Groundwater, Magnetotellurics, Self-Potential.

TABLE OF CONTENTS

LIST OF FIGURES AND TABLES

INTRODUCTION

Coal Seam Gas (CSG) production relies on the extraction of water from coal seams to allow flow and capture of natural gas in a process called depressurisation. This process is unavoidable when unlocking the resource potential of a CSG resource. The removal and management of CSG water is a critical responsibility of the involved parties. Water extraction can continue for up to approximately 15 years, dependent on the geological formation of the base (Day 2009). In 2007, 12.5 GL of CSG were extracted in Queensland alone (Cox 2013). At current growth rates, it is estimated that Surat Basin will produce an annual average of 25GL of CSG water for the next 25 years due to demand of the Australian and international markets (Nghiem et al. 2011).

Current industry standards in groundwater monitoring for CSG projects use water sampling at observation boreholes to identify water table movement and groundwater interaction using geochemical signatures of CSG water (Taulis and Milke 2013). This an expensive technique requiring drilling that can only provide point information. Microseismic monitoring is used in deeper unconventional shale gas plays to detect creation of fracture networks caused by hydro-fracture stimulation, however it is not directly sensitive to associated groundwater movement and is still being evaluated for CSG monitoring potential (Compagnie Générale de Géophysique 2013). However, there is still no consensus monitoring method for assessing the impact of CSG projects in extended groundwater networks (Australian Government National Mesurement Institute 2013). Due to increasing public concern and government pressure for regulation of CSG groundwater monitoring, the development of new efficient monitoring techniques is in high demand within the industry.

This paper provides a first stage feasibility study for the use of electromagnetic (EM) magnetotelluric (MT) methods, and electrokinetic (EK) self-potential (SP) methods to

capture surface data for mapping and monitoring the short and long term changes of sub-surface groundwater distribution in a CSG depressurisation program.

Neither MT nor SP methods have been applied to any aspects of CSG production, and therefore their monitoring potential is yet to be assessed Previously, MT monitoring has been successfully applied to deeper geothermal resources, but these processes have not been applied to monitoring changes in the top 1 km of Earth (Peacock et al. 2012). Combined with other geophysical methods, SP surveys are especially useful for locating and quantifying groundwater flows and estimating hydraulic properties of aquifers, including water table depth and hydraulic conductivity (Jouniaux et al. 2009).

If proven successful, the combination of large scale (km) long-term MT and localised (~250 m) live-feed SP fluid-flow monitoring have the potential to become a standardised technique for CSG resource capture and environmental monitoring.

Improved monitoring of coal seam depressurisation can provide clarification of gas capture zones surrounding a CSG well, uncovering a seam's full gas resource potential and preventing drilling of overlapping dry wells. Monitoring can also detect the occurrence of potentially hazardous environmental groundwater implications associated with CSG fracking and depressurisation operations.

This study is a feasibility introduction of background, technique and equipment testing to arouse industry and public interest, and is split in three parts: 1.) a synthetic study which assesses the ability of an MT array to detect resistivity changes caused by the depressurisation of a coal seam.; 2.) a SP model study in which the hydrological problem is first solved, and then the depressurisation electrical potential is computed; and finally, 3.) a MT and SP field trial undertaken on-site an aquifer injection scheme to determine the

electrical noise characteristics and ability of the instruments to measure sub-surface fluids, in particular the effectiveness of the prototype SP logger design.

BACKGROUND THEORY

Magnetotelluric Theory

Magnetotelluric methods are sensitive to the electrical conductivity of the subsurface. Natural-source broadband MT has been shown to effectively determine orientation of fluid propagation in a deep (3.8 km) geothermal engineered injection system (Peacock et al. 2012). At shallower depths of below 500 meters, audio MT (AMT) and controlled source AMT has greater data resolution and has been used in pilot studies for CO_2 sequestration monitoring, and gas field developments (Streich et al. 2010, Hördt et al. 2000).

Electromagnetic methods in general are at present an underutilised tool for sub-surface fluid mapping, with MT methods predominately used as a geothermal and economic anomaly exploration tool (Revil et al. 2012, Heise et al. 2008, Spichak and Manzella 2009). The recent successful application of MT monitoring in Peacock et al., (2013) maps fluid propagation in deep shale engineered systems and provides a great foundation of monitoring success to expand upon. There are several contrasting factors that differentiate our feasibility study from previous successors, including: MT monitoring has never been applied to a depressurising coal seam and its results are therefore unpredictable; the monitoring area is shallower at approximately 500 m depth with far greater aquifer connectivity; the physical conditions of a coal seam are more ductile and elastic than brittle, deep shale conditions; and finally, monitoring transition of conductive to resistive sub-surface, compared against resistive to conductive sub-surface.

Magnetotellurics is a passive technique that measures Earth's electrical response to a broad spectrum of naturally occurring and diffusive geomagnetic variations, formally linked by the linear MT transfer function $\boldsymbol{Z}$ in frequency domain (Simpson and Bahr 2005):

$$\begin{pmatrix} E_x \\ E_y \end{pmatrix} = \begin{pmatrix} Z_{xx} & Z_{xy} \\ Z_{yx} & Z_{yy} \end{pmatrix} \begin{pmatrix} B_x \\ B_y \end{pmatrix} \quad (1)$$

where components are measured for electrical field $\boldsymbol{E}$, which is voltage difference measured with dipoles between two electrodes (north and east), and the inducing magnetic field B (given by orientations x and y) which is essentially the primary input measured with induction coils (time change). The tensor $\boldsymbol{Z}$ has four complex components in the frequency domain that describe the relationship between $\boldsymbol{E}$ and $\boldsymbol{B}$ at any period. In a three-dimensional environment all the components of the electric and magnetic field are linked to each other; the impedance tensor or MT transfer function Z links the corresponding horizontal components. Magnetotelluric depth of investigation and resolution depends directly on the periodicity (T) of the source as well as the resistivity distribution ρ of the subsurface (Kaufman and Keller 1981). The simplified skin depth equation:

$$\delta_a \approx 500\sqrt{\rho_a T} \quad (2)$$

summarises total potential depth of investigation (δ_a) or accounting for exponential decay of electromagnetic fields as they diffuse into a medium (Simpson and Bahr 2005). To solve the depth weighted average apparent resistivity distribution for ρ orthogonal (Equations 3 a and 3 b), where a higher average resistivity results in a greater depth of investigation:

$$East\ electric\ dependent: \rho_{a_{xy}} = 0.2T \left|\frac{E_x}{B_y}\right|^2 = 0.2T \left|Z_{xy}\right|^2 \quad (3\ a)$$

$$North\ electric\ dependent: \rho_{a_{yx}} = 0.2T \left|\frac{E_y}{B_x}\right|^2 = 0.2T \left|Z_{yx}\right|^2 \quad (3\ b)$$

Also used to define sub-surface structure is difference in wave phase (ϕ) between inducing field B, and the induced field $\boldsymbol{E}$ given by:

$$\phi_{xy} = \arctan\left(Z_{xy}\right) \quad (4\ a)$$

$$\phi_{yx} = \arctan\left(Z_{yx}\right) \quad (4\ b)$$

This study will concentrate on mapping spatial change in ***E*** (Earth's electric response) due to temporal changes in ***Z*** (Earth's filter) caused by dewatering (and associated increase of resistivity) of a coal seam.

Self-Potential Theory

The SP method is a passive geophysical method involving the measurement of the electrical potential distribution at a set of measurement points (stations). The measurements are performed using non-polarizing electrodes, and the difference of the electrical potential between electrodes is measured by using a voltmeter with a high sensitivity (at least 0.1 mV) and a high input impedance (typically in the range 10–100 MΩ for soils) (Revil et al. 2012). SP mapping at the ground surface uses a reference electrode (or grounding probe) as a fixed base to monitor change of electrical potential signal in the surveys electrodes (Petiau 2000).

Movement of groundwater within a reservoir has long been known to produce a measureable SP signal due to the electrical interactions of ions with matrix materials (Ishido and Pritchett 1999, Ishido and Mizutani 1981, Revil et al. 1999, Knight et al. 2010). Moreover, SP may be the only geophysical technique that specifically measures fluid dynamics, but its uptake to industry has been limited due lack of exposure, temperature and moisture effects, and resolution (Birch 1993).

In the last few years, the technique has gained importance particularly where pumping tests such as coal seam depressurisation introduce a measureable change in the Earth (Rizzo et al. 2004, Malama et al. 2009, Malama et al. 2008). SP monitoring is used mainly for near

surface (top 100 meters) conditions, but has not been readily applied to depths of approximately 500 m for the recovery of a CSG resource.

Streaming potentials or EK potentials are caused by the motion of ions with the flow of a liquid. In a system consisting of two separate phases such as liquid and a solid medium, there has to be a electro-neutral total balance of charge (Fagerlund and Heinson 2003). Passive electrical currents, and therefore SP signals are generated through an electrical double layer at the pore-water/mineral interface. When minerals such as silica are in contact with groundwater that contains dissolved ions, the mineral grain surface becomes electrically charged due to chemical reactions between the surface sites and the pore water (Figure 1). The change distribution results in the formation of a diffuse layer characterized by an excess of counter ions and a depletion of co-ions. In addition, some ions can be sorbed directly on the mineral surface forming the so called Stern Layer (Revil and Florsch 2010).

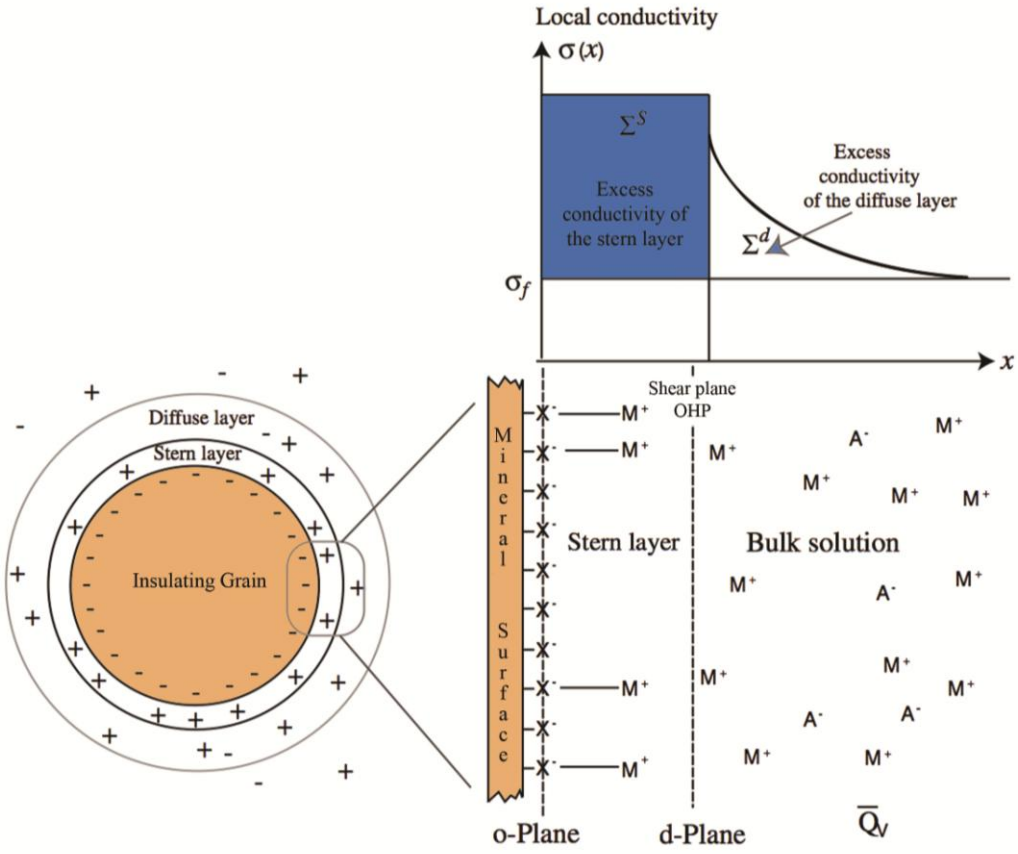

Figure 1: Sketch of distribution of the ionic species in the pore space of a charges porous medium at equilibrium. Pore water is characterized by a volumetric charge density $\overline{Q_V}$, corresponding to the charge of the diffuse layer per unit pore volume (in C m^{-3}). The Stern layer is responsible for the excess surface conductivity $\sum^{S}$ (in S) with respect to conductivity of the pore water σf, while the diffuse layer is responsible for the excess surface conductivity $\sum^{D}$. The Stern layer is located between the o-plane (mineral surface) and the d-plane, which is the inner plane of the electrical diffuse layer. The diffuse layer extends from the d-plane into the pores (adapted from Revil and Florsch 2010).

The electrical double layer, which is crucial for the generation of streaming potentials, can be described by models of various complexities. Assuming that 1.) the flow is laminar and 2.) the radius of curvature of the capillary or pore is much bigger than the thickness of the double layer, the convective electric current per unit area, i_{conv}, over a capillary or pore is given by Equation 5 (Revil and Florsch 2010):

$$i_{conv} = \frac{\zeta \varepsilon_r \varepsilon_0}{\eta} \overline{\nabla_{\mathrm{n}} P} \tag{5}$$

Where $\zeta$is the ζ- (zeta) potnetial, ε_r is the relative dielectric contant of the liquid and ε_0 is the dielectric constant of vacuum, η is the viscosity of the fluid and $\overline{\nabla_{\mathrm{n}} P}$ is the mean pressure

gradient normal to the cross-section area (Overbeek 1952). Note that since fluid flows in direction of negative pressure gradient ($-\nabla P$), and as ε_r, ε_0 and η are positive constants, if $\zeta$is negative, than i_{conv} is positive in the direction of flow, and there is a resultant transport of positive charge ions with flow.

As consequence of the convection current, an electric potential gradient (streaming potential) is established along the flow path. Potential gradient causes current to flow back through the liquid by electrical conduction. The conduction current per unit area, i_{cond} , over a cross section is given by Ohm's law (Fagerlund and Heinson 2003):

$$i_{cond} = -\sigma\overline{\nabla_{\mathrm{n}} V} \tag{6}$$

Where σ is the bulk conductivity of the liquid, and $\overline{\nabla_{\mathrm{n}} V}$ is potential gradient normal to the cross section. In the absence of external current sources the total current is the sum of the convective and conductive currents, $i_{total} = i_{conv} + i_{cond}$. For steady-state conditions the convective current produced by fluid flow is balanced by the return conduction current, $i_{cond} = i_{conv}$, and the total current equals zero . Combination of Equation 5 and Equation 6 results in a directly proportional relationship between $\overline{\nabla_{\mathrm{n}} V}$ and $\overline{\nabla_{\mathrm{n}} P}$ represented by Equation 7, known as the Helmholz-Smoluchovsky equation (Helm 1987):

$$\overline{\nabla_{\mathrm{n}} V} = \frac{\varepsilon_r \varepsilon_0 \zeta}{\eta\sigma}\overline{\nabla_{\mathrm{n}} P} = C_S\overline{\nabla_{\mathrm{n}} P} \tag{7}$$

where $C_S = \varepsilon_r \varepsilon_0 \zeta/\eta\sigma$ is the streaming potential coupling coefficient that links the fluid pressure to the self-potential voltages established.

Groundwater flow is driven by the hydraulic head gradient, ∇H, rather than ∇P. As $P = \rho g H$, where ρ is the density of the fluid (in kg/m^3), g is the specific gravity (9.81 m/s^2) and H the hydraulic head, written as (Fagerlund and Heinson 2003):

$$\overline{\nabla_{\mathrm{n}} V} = \frac{\varepsilon_r \varepsilon_0 \zeta \rho g}{\eta \sigma} \overline{\nabla_{\mathrm{n}} H} = C_S' \overline{\nabla_{\mathrm{n}} H} \tag{8}$$

Thus, the streaming potential gradient is proportional to the pressure gradient, and in a controlled laboratory environment Equation 7 and 8 are excellent determinants for C_S and ζ.

In models relating streaming potentials to groundwater flow, groundwater flow can be regarded as the primary flow producing the secondary electric current flow. The two flows are interdependent and referred to as coupled (Fagerlund and Heinson 2003). The effect of current flow on groundwater flow (electro-osmosis) can, however, safely be neglected for normal rock-water systems(Sill 1983, Fitterman 1978, Ishido and Pritchett 1999). Ground water flow can normally be described by Darcy's Law (Todd and Mays 1980);

$$\frac{Q}{A} = -\frac{k}{\eta} \nabla P = -\frac{kg\rho}{\eta} \nabla H = -K \nabla H \tag{9}$$

where Q is the fluid flux (volume/time), A the cross-section area, k the intrinsic permeability (in m^2), and K the hydraulic conductivity (in m/s). $Q/A = v$ is the Darcy-velocity in m/s.

A simple model of the groundwater flow towards a production well within an unconstrained aquifer can be obtained with the following assumptions (Fagerlund and Heinson 2003):

1. Darcy's law holds.
2. The aquifer is homogenous, isotropic and of infinite areal extent.
3. The piezometric surface before pumping is horizontal.
4. The well fully penetrates the aquifer, which is bounded by a horizontal confining bottom.
5. Water is instantaneously removed from storage upon a decline in head.
6. Steady-state conditions have been reached, that is, drawdown does not change with time.

For an unconfined aquifer, groundwater flow towards a production well under these assumptions can be described by Thiem's equation (Bear 1979, Fetter 1994) which is given by:

$$H_2^2 - H_1^2 = \frac{Q}{\pi K} \mathrm{L}n \left(\frac{r_2}{r_1}\right) \quad (10)$$

Where H_1 and H_2 are the heads at radial distances r_1 and r_2 from the production well respectively. Note that the drawdown $= H_0 - H$, where H_0 is the head before pumping, and the hydraulic head is equal to the saturated thickness of the aquifer.

A simple model of the groundwater flow to estimate water produced by individual wells within a confined aquifer that is homogenous, isotropic and of infinite extent can represented by the Theis equation (Driscoll 1986, Fetter 1999, Domenico and Schwartz 1998);

$$s = \frac{Q}{4\pi T} W(u) \quad (11)$$

Where s is drawdown quantified by the amount of decline in groundwater level caused by pumping, Q is well production or pumping rate applied, T is transmissivity which is a hydrogeological measure of the ability of an aquifer to transmit water and $W(u)$ is the well function, which is an indicator of steady-state groundwater flow.

When applying Theis' equation (Equation 10) to a CSG project the confined conditions assumption is important and is supported by the operational approach to depressurise and not completely dewater an aquifer, thus a remnant head on the producing coal seam is maintained, which in turn maintains the confined nature of the producing zone (Klohn Crippen Berger Ltd 2012).

SYNTHETIC MODELLING STUDIES

With the possibility of further on-site CSG monitoring feasibility studies within South Queensland's Surat Basin, Walloon Coal Measures, synthetic models are based on its basic geological model and its current average CSG project pumping conditions.

The Surat Basin comprises many different geological layers including mainly sandstone, mudstone and siltstone. The sandstones act as permeable aquifers, whilst the mudstones and siltstones that comprise coal measures are relatively impermeable aquitards (Exon 1976). The coal seam formations are discrete and discontinuous over large distances; generally, they form only 10% of the total thickness of the coal measures and range between 20- 50 m. These formations are generally located between 200- 1000 m below sub-surface (Australia Pacific LNG 2013).

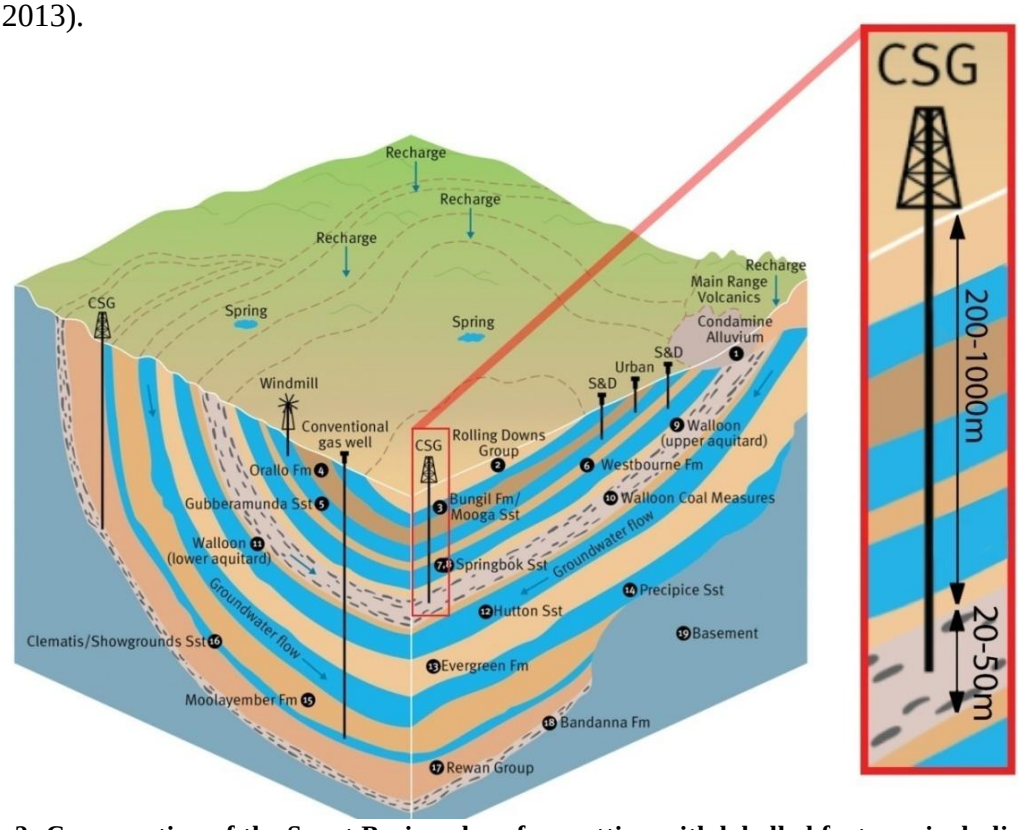

Figure 2: Cross section of the Surat Basin subsurface setting with labelled features including: formations (Fm); sandstones (Sst); geological groups; aquitards; basement depth; groundwater flow zones; coal measures, and various bore types and their relative depths. A Walloon Coal measure CSG well is featured in the red zoomed window. The profile displays range of typical sub-surface and coal measure depths (adapted from Cox 2013).

Magnetotelluric Modelling

Synthetic Surat Basin CSG models were created for analysis of the MT geophysical technique. Two scenarios where processed under identical software modelling conditions simulating the pre- and post- depressurisation subsurface conditions of a CSG site:

Pre- depressurisation commencement (1-D) (Figure 4 a):

The surface begins at 30 Ωm resistivity and slowly decreases to a minimum resistivity of 1 Ωm at 600 m depth. At 600 m depth the profile begins to increase resistivity rapidly, reaching a final maximum resistivity of 100 Ωm at 3500 metres depth.

Post-depressurisation gas recovery commencement (3-D)(Figure 4 b):

The CSG depressurisation process causes a localised and contained increase of resistivity value over depths of 500 m to 550 m depth from 1 Ωm to 1000 Ωm. The increased resistivity coal seam expands laterally a total of 1500 m, and is centralised to the model and MT surface station 13.

50 MT surface stations where arranged with 250 m spacing in two equal lines of north-south and west-east orientations (Figure 3). The lines intersect centralised to the depressurising coal seam at stations 13 (west-east) and 38 (north-south). Two-dimensional (2D) forward MT modelling was undertaken on the synthetic canonical models (Figure 4). Using methods described in Mackie et al., (1993) a forward calculation was set at 100Hz to 0.1Hz frequency range over 4 decades, 3 periods per decade. Settings used were to solve for the smoothest model inversion including a uniform grid Laplacian operator, and Tau for smoothing operator at a value of 50.

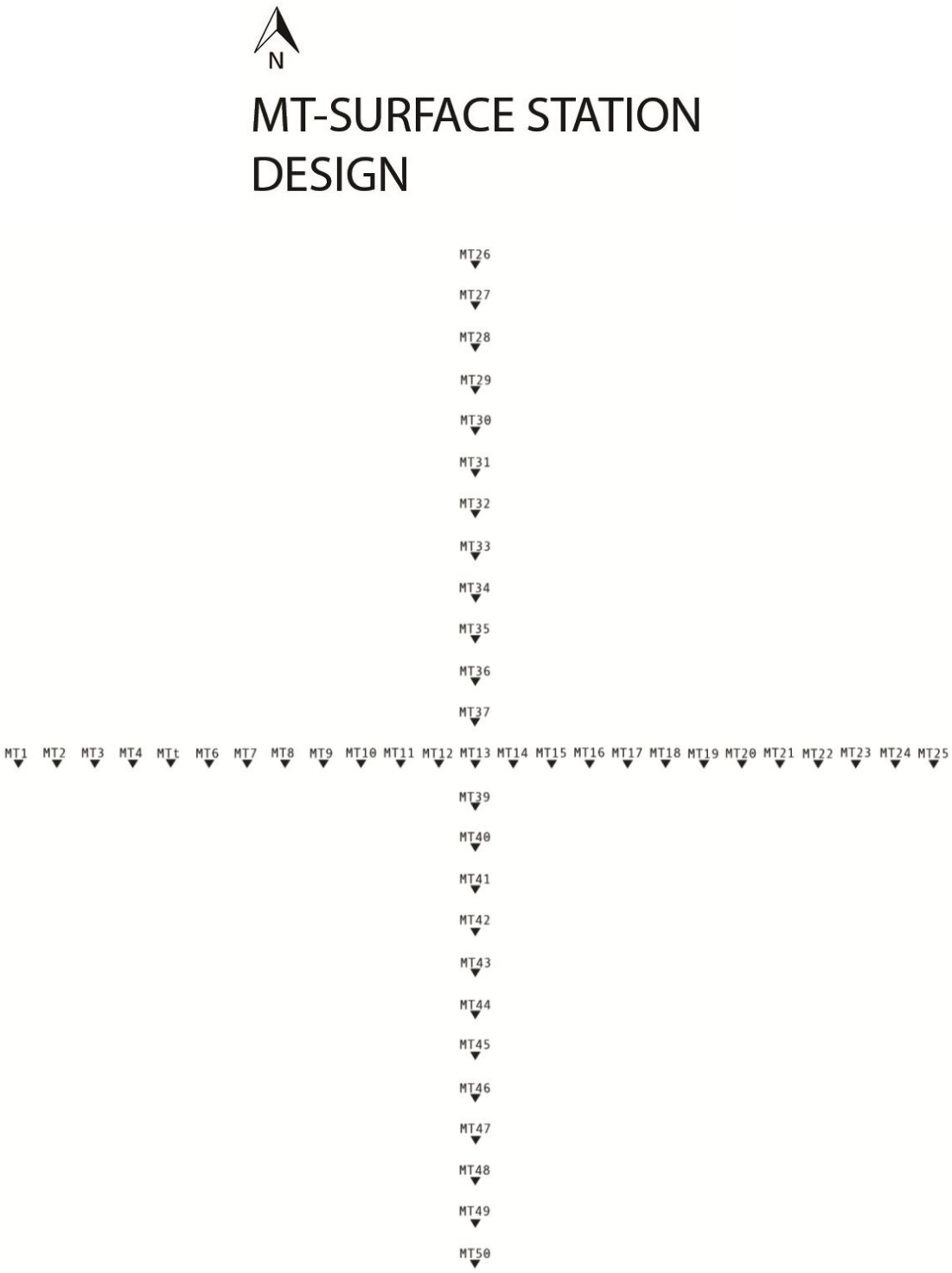

Figure 3: Surface design of MT stations for synthetic feasibility models Pre-depressurisation and Post-depressurisation. The design utilizes 49 monitoring stations (central MT13 overlaps central MT38) with 250 m spacing between stations. The straight profile design was used in favour of an evenly distributed grid to maximise data capture for a straight-line 2-D inversion of the CSG depressurisation event.

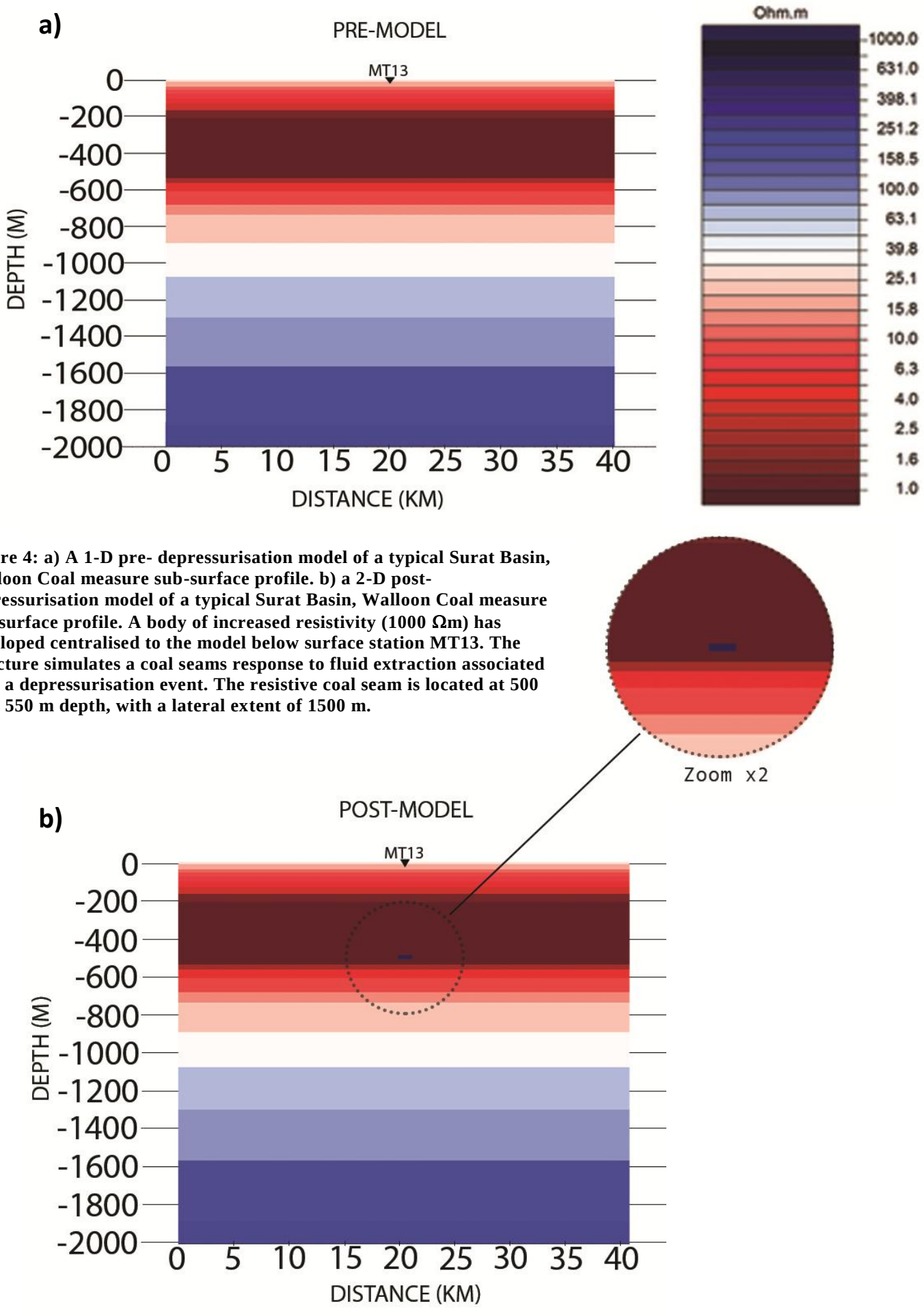

Figure 4: a) A 1-D pre- depressurisation model of a typical Surat Basin, Walloon Coal measure sub-surface profile. b) a 2-D post-depressurisation model of a typical Surat Basin, Walloon Coal measure sub-surface profile. A body of increased resistivity (1000 Ωm) has developed centralised to the model below surface station MT13. The structure simulates a coal seams response to fluid extraction associated with a depressurisation event. The resistive coal seam is located at 500 m to 550 m depth, with a lateral extent of 1500 m.

Self- Potential Modelling

Two scenarios of models where processed under identical software modelling conditions simulating the beginning to early and late to ending depressurisation recovery stage conditions of a CSG resource:

SP1: Beginning-Early Depressurisation (Figure 6 a):

Pumping at 510 m depth with a typical pump rate of 20,000 L/day (Cox 2013), depressurising a 20 m coal seam at 5 Ωm resistivity and 10 milliDarcies= 10^{-14} m^2 permeability. High hydraulic conductivity values are present within the coal; all hydraulic conductivity values outside of the seam are two orders of magnitude higher (Figure 6 a) therefore fluids are much less likely to flow external to the coal seam. Neumann boundary conditions were applied on the model top and bottom sides and a zero imposed hydraulic head on the model sides (as the model sides are far from the pumping area). Neumann conditions of constant gradient imply no flow out of the model.

SP2: Late-Ending Depressurisation (Figure 6 b):

All model parameters set are identical to SP1. Although, due to gradual fluid loss caused by depressurisation of the coal seam, resistivity of the 20 m coal seam aquifer has increased by a factor of 10 to equal 50 Ωm.

Calculations were undertaken using the 2D modelling code ‘SP2DINV’ constructed by Soueid Ahmed et al., (2013). In this code the fluid flux is initially solved, and using a cross-coupling coefficient from the coal resistivity and dielectric properties a resulting SP voltage is calculated (Figure 5).

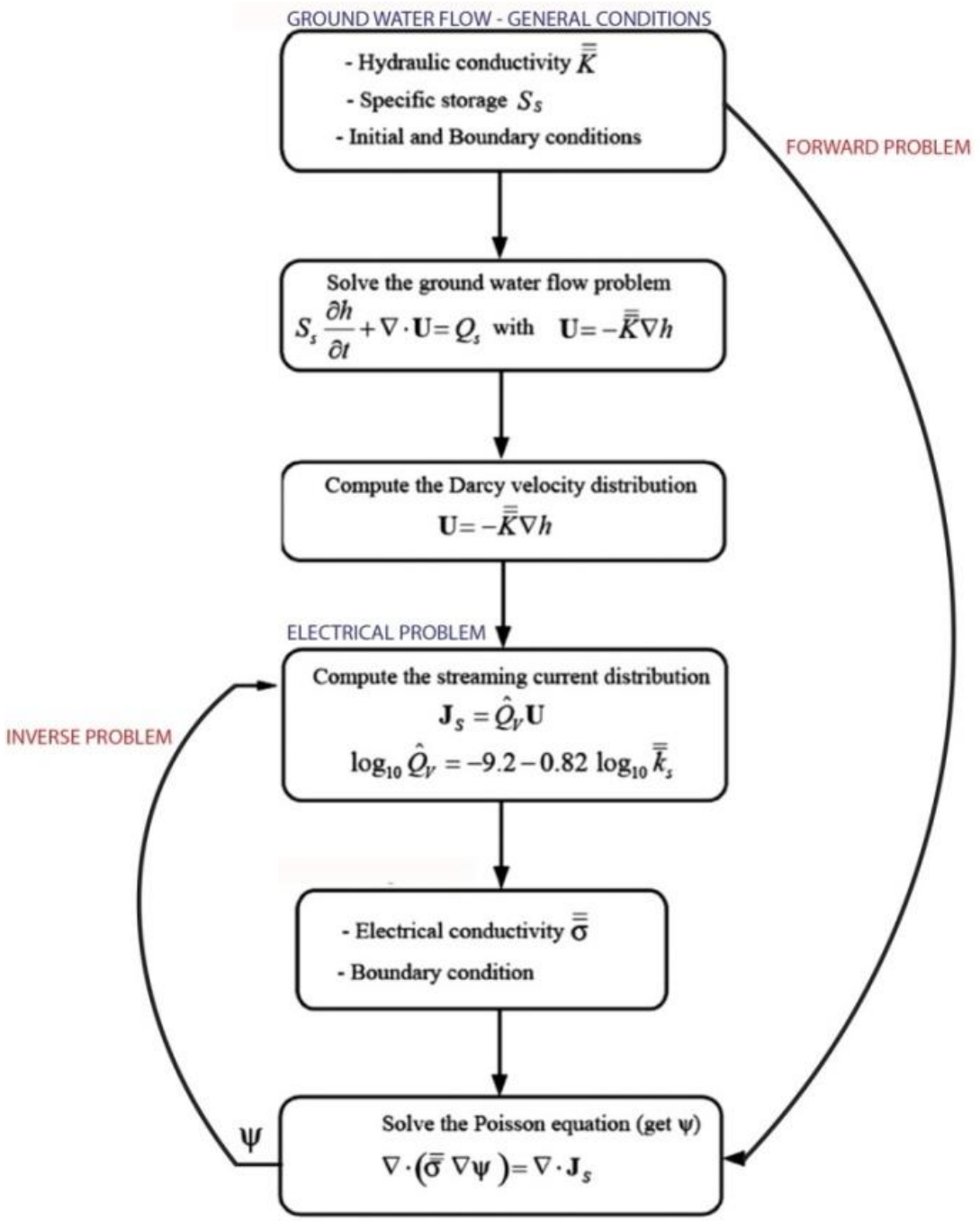

Figure 5: Flowchart for the simulation and inversion of the self potential data associated with ground water flow. Vector fields U and J_s denote the Darcy velocity and the source current density, respectively; and potentials *h* and ψ denote the hydraulic head and the electrical potential, respectively. In saturated conditions, the material properties entering the forward modelling are the hydraulic conductivity and electrical conductivity tensors, and the specific storage coefficient (Soueid Ahmed et al. 2013).

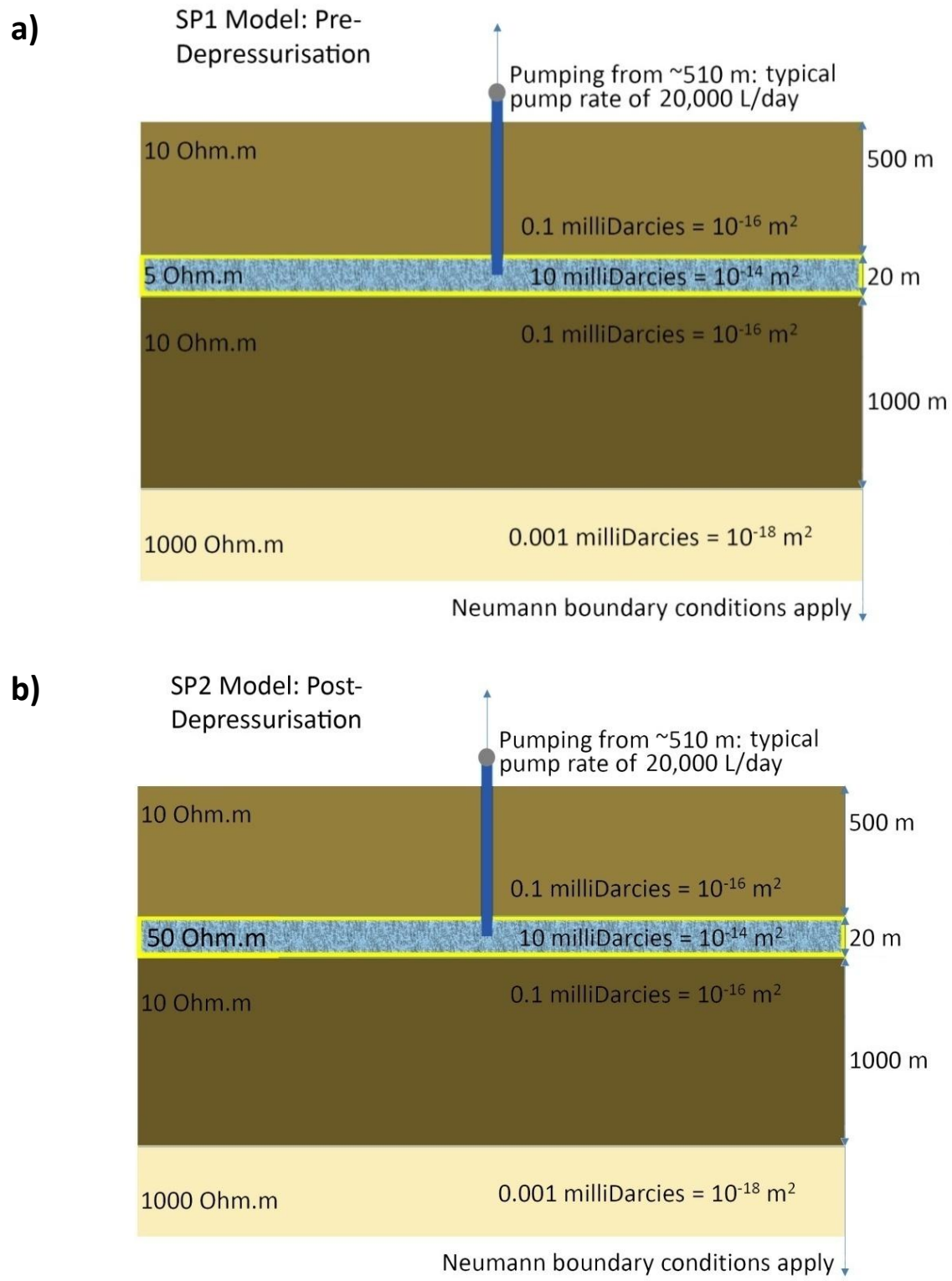

Figure 6: a) SP1 pre- depressurisation model of a typical Surat Basin, Walloon Coal measure sub-surface profile. The 5 Ωm 500 m to 550 m depth band represents the targeted coal measure resource (yellow) that will undergo depressurisation b) SP2 post-depressurisation model of a typical Surat Basin, Walloon Coal measure sub-surface profile. An increased 50 Ωm resistivity has developed at 500 m to 550 m simulating the coal seams (yellow) response to fluid extraction associated with a depressurisation event

SYNTHETIC MODELLING RESULTS

Magnetotelluric Modelling Results

From the 1-D and 3-D model, a 2D line of surface sites in west-east orientation (MT1 to MT25) centralised to the resistive coal seam were extracted. The west-east surface line data are inverted for a 2D structure so a comparison can be made from the 2D inversion of pre- and post- depressurisation models (Figure 7).

Within the 2-D post-depressurisation inversion (Figure 7 b), resistivity increases at 500 m to 550 m depth band underlying stations MT11 to MT16 are consistent with input post-deperssurisation model (Figure 4 b). However, an increased resistivity induced by the highly resistive depressurised coal seam is evident from approximately 400 m to 1000 m depth, inconsistent with input model data.

Pseudosections of the 2D post-depressurisation inversion (Figure 8) show changes in apparent resistivity and phase for the two modes of induction (TE and TM). In TE & TM phase plots, a change in the 0.1 to 0.3 S period range is observed representing a change of sub-surface structure caused by the introduction of the higher resistivity coal seam body. In TE & TM Rho (resistivity) plots, change is pronounced over a much broader 0.2 S to 100 S period range.

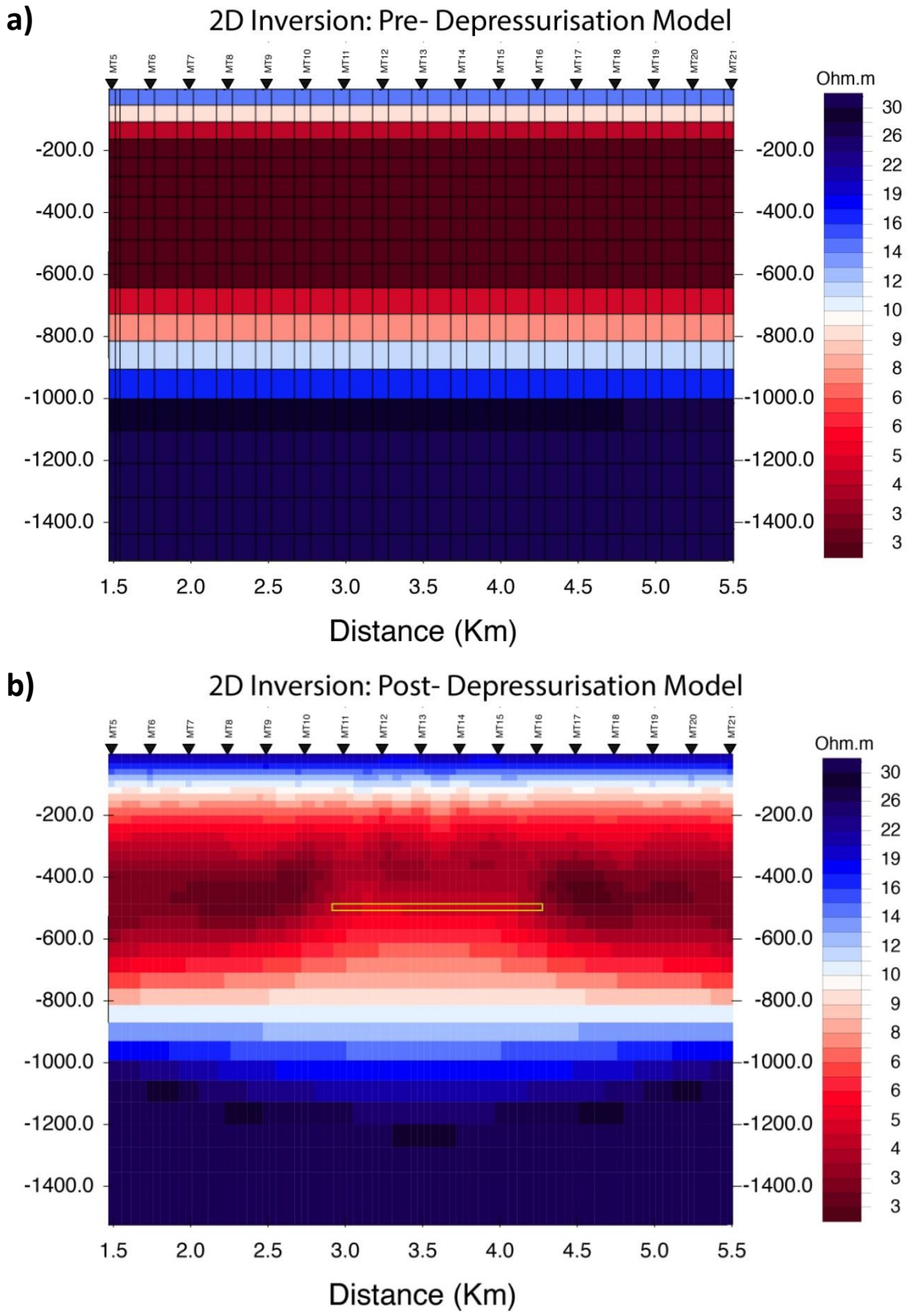

Figure 7:a) 2D Inversion of pre-depressurisation input model for stations MT5 to MT21, west-east transect. b) 2D Inversion of post-depressurisation input model for stations MT5 to MT21, west-east transect. Highlighted in yellow is the true input model location of the increased resistivity (1000 Ωm) depressurised coal seam. Inversion settings were set to solve for the smoothest model inversion, including a uniform grid Laplacian operator, and Tau for smoothing operator at a value of 50.

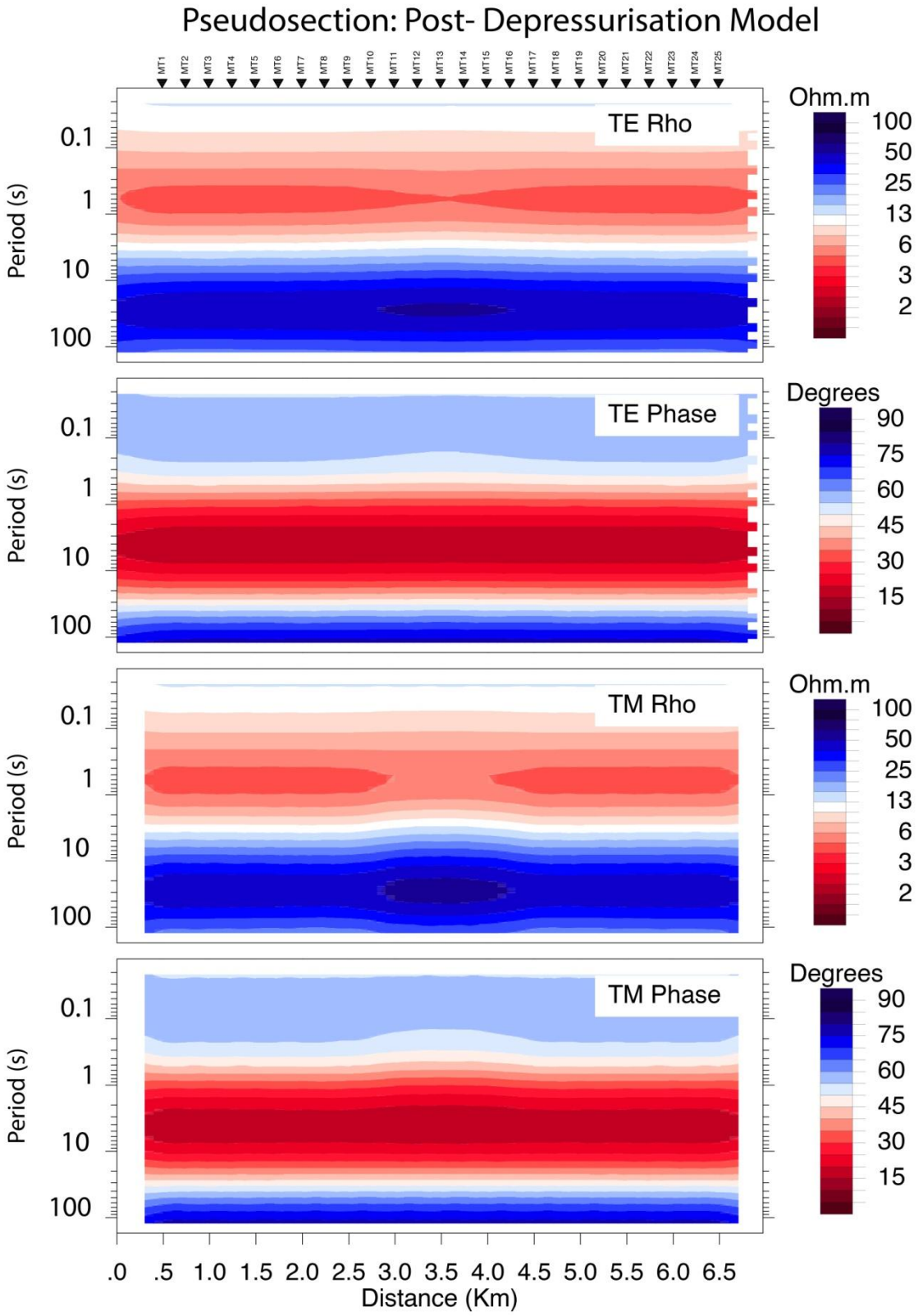

Figure 8: Pseudosection of post-depressurisation model, stations M1-M25 in west-east transect. Highly resistive (1000Ωm) coal seam structure at 500 m to 550 m depth is expected to produce measurable changes in TE & TM Rho at ~1 s, and in TE & TM Phase at ~0.2 s. Inversion settings were set to solve for the smoothest model inversion, including a uniform grid Laplacian operator, and Tau for smoothing operator at a value of 50.

Self-Potential Modelling Results

Hydraulic head (Figure 9) is the water pressure that drives the fluid flow during coal seam depressurisation. However, actual flow of sub-surface fluid depends on combined hydraulic head pressure and hydraulic conductivity of the subsurface. Hydraulic head is consistent for both SP1 and SP2 models (Figure 6) as it is unaffected by changes in sub-surface resistivity. The high hydraulic head will yield low flow in zones external to the coal where the hydraulic conductivity is two orders of magnitude higher. The hydraulic head (Figure 9) value is highest localised around the coal seam extraction pump, reaching a maximum value of 38,000 m. Within a 1,000 m lateral radius of the extraction pump, hydraulic head within the depressurising coal seam remains high between 35,000 m to 25,000 m. The hydraulic head value decreases at approximately 1,000 m per 100 m distance from the fluid extraction pump, until reaching a value of approximately zero at 4 km distance from extraction pump.

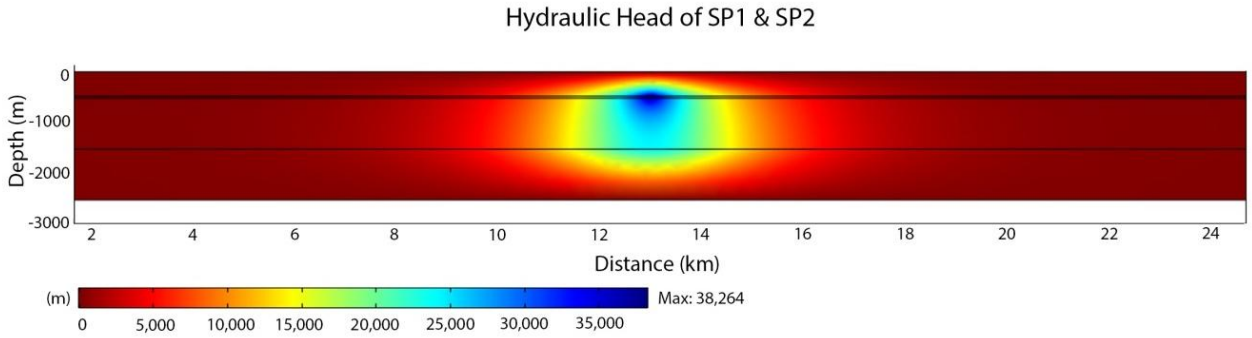

Figure 9: Surface hydraulic head pressure (m) of SP1 (pre-depressurisation) and SP2 (post-depressurisation) models. Calculations were undertaken by 2D modelling code SP2DINV (Soueid Ahmed et al. 2013) (adapted from figure prepared by A. Jardani 2013).

The electric potential of the SP1 model (Figure 10) reaches its maximum value of approximately 20 mV localised around the coal seam fluid extraction pump, and approximately 13mV at the surface directly above pumping location. Note that these potentials are effectively the voltage relative to a zero potential several kilometres from the borehole. Electrical potentials decrease at a rate of approximately 2.5mV per 1 km, and is measurable at the surface for approximately 5 km either side of the fluid extraction pump.

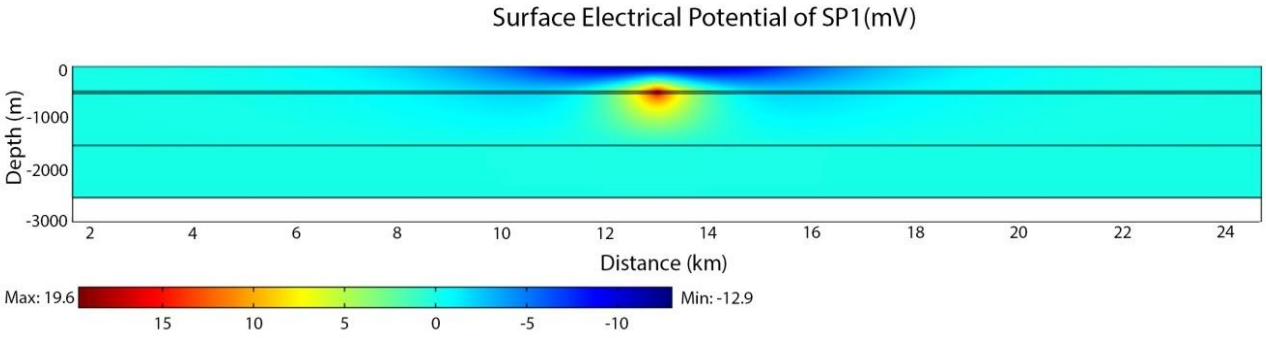

Figure 10:Surface Electric Potential (mV) of SP1 (pre-depressurisation) model with calculations undertaken by 2D modelling code SP2DINV (Soueid Ahmed et al. 2013) (adapted from figure prepared by A. Jardani 2013).

When resistivity of the coal seam increases by a factor of 10 due to depressurisation effects, a subsequent increase in electric potential signal is evident. The electric potential of the SP2 model (Figure 11) reaches its maximum value of 200 mV localised around the coal seam fluid extraction pump, and approximately 130mV at the surface directly above pumping location. Electrical potential value decreases at approximately 25mV per 1 km, and is measurable at the surface for approximately 5 km either side of the fluid extraction pump.

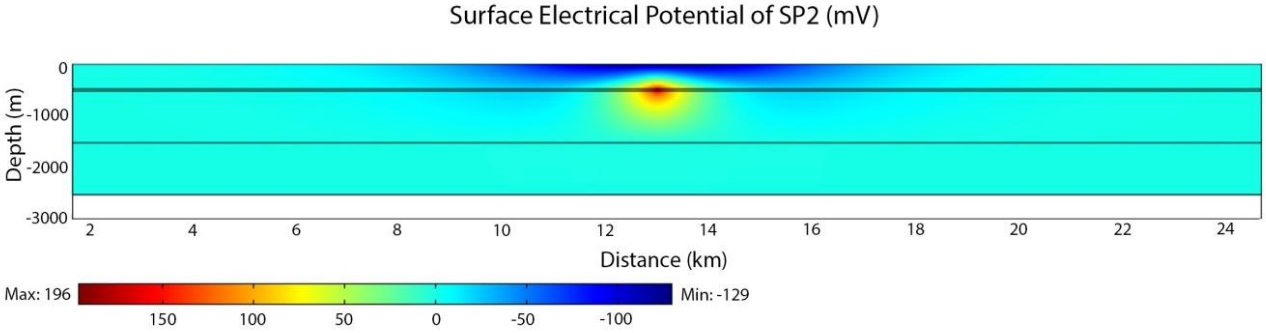

Figure 11: Surface Electrical Potential (mV) of SP2 (post-depressurisation) model with calculations undertaken by 2D modelling code SP2DINV (Soueid Ahmed et al. 2013) (adapted from figure prepared by A. Jardani 2013).

FIELD INSTRUMENTATION STUDIES

Survey and Site Analysis

A monitoring program was conducted on-site of the SA Water Adelaide Airport Aquifer Injection Scheme Project, South Australia. The project uses aquifer injection and extraction bores to harvest stormwater into a major subsurface storage basin for on demand reuse. The site was used as it was a local project of relative resemblance to a CSG depressurisation event that also uses extraction bores to interact with subsurface fluids. The operative groundwater injection and extraction bores are due south-west of the survey site.

The injection and extraction bores are 160 m depth, with pumps at 100 m depth. The loggers were set-up within 250 m of operative injection and extraction bores; loggers could not be located closer to the bore due to area restraints. This range was perceived as sufficient to still receive a measurable SP voltage signal generated by engineered sub-surface fluid pumping.

The field survey was programmed to capture three days (72 hours) of continuous MT and SP data to detect averaged variation within the site area.

Magnetotelluric Field E-Logger

MAGNETOTELLURIC FIELD LOGGER SURVEY:

The Adelaide University E-Logger stations (L1, L25 and L28) effectively collected MT data on-site of the Adelaide airport stormwater injection scheme. All E-Logger stations on site recorded stable and consistent data.

Raw data collected had identical and within phase signals for east and west channels. North and south channel signals had an underlying harmonic oscillation and no data correlated, however they appeared to be within phase (Figure 12 a). Clear peaks of noise at the 4 Hz and

50 Hz frequency ranges are visible in the raw data amplitude spectrum (Figure 12 b). Width of the frequency peaks ranged amongst loggers between 1 Hz to 4 Hz. The high noise signal within the north and south channels were frequently of equal amplitude to correlating events in the east and west channels.

Filtering effects were applied to raw data to minimise noise influence particularly affecting north and south stations (Figure 13 a). A 8 Hz highpass filter was applied to filter the 4 Hz noise, and a 4 Hz width notch filter including harmonics was applied at 50 Hz.

Frequent occurrences of unidentified patterned events were recorded in east west channels of all loggers, however north and south channels detected no recognisable event (Figure 13 b). Events were one-second pulsations over 45 s repeating after 2 minute breaks.

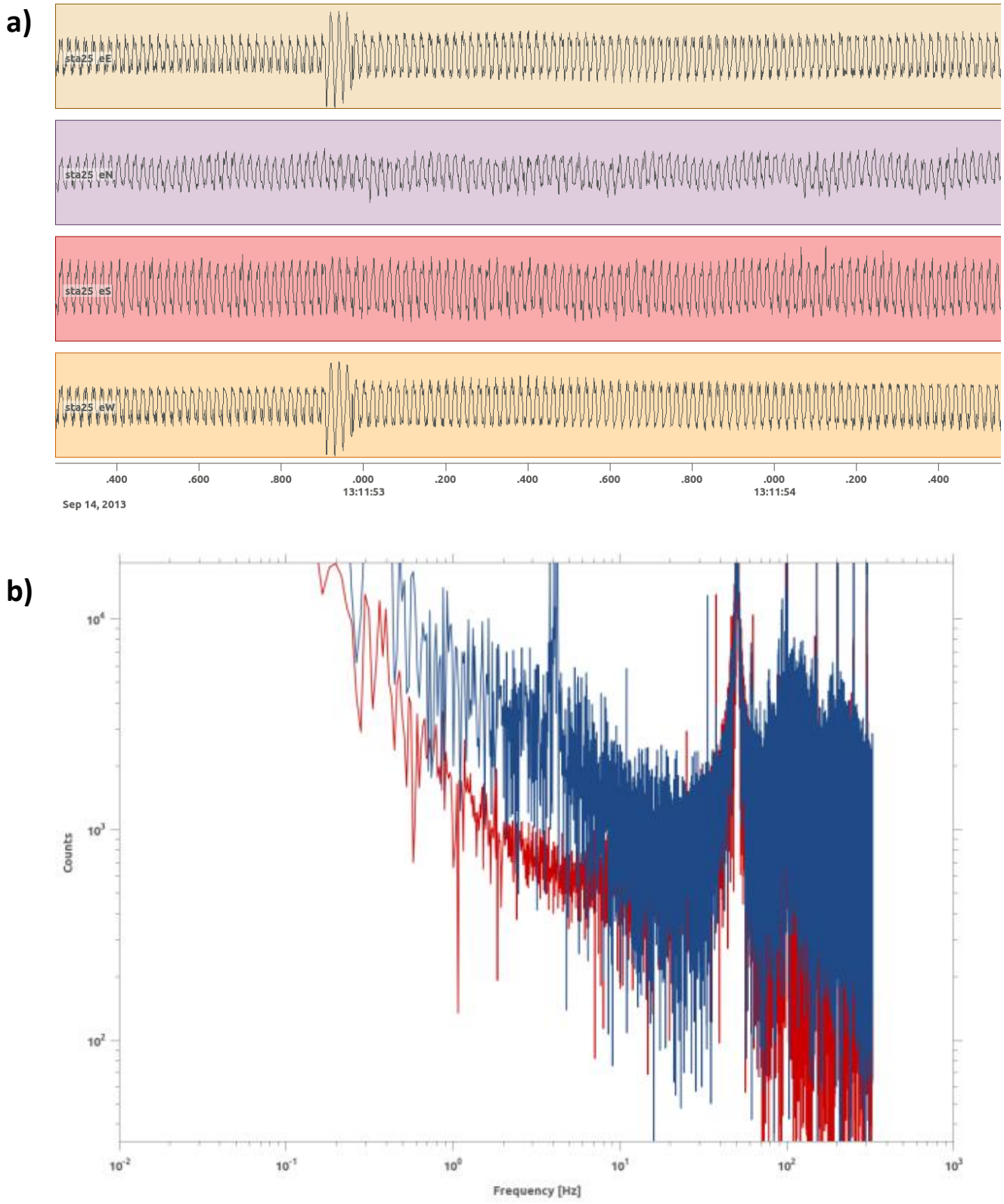

Figure 12: MT e-logger on-site monitoring of Adelaide Airport Aquifer Injection Scheme. Conducted from 13 to 16th September 2013. Testing was conducted in a heavily urbanised setting, within 1 km distance of Adelaide Airport. a) A ~2 s window time series of raw data from station 25. The time series gives a typical profile of the raw data obtained from all three stations. A high noise signal in north and south channels with an underlying harmonic oscillation and no correlating data. b) Station 1 amplitude spectrum with visible peaks of noise at the 4 Hz and 50 Hz frequencies. All three stations recorded similar overall amplitude spectrums.

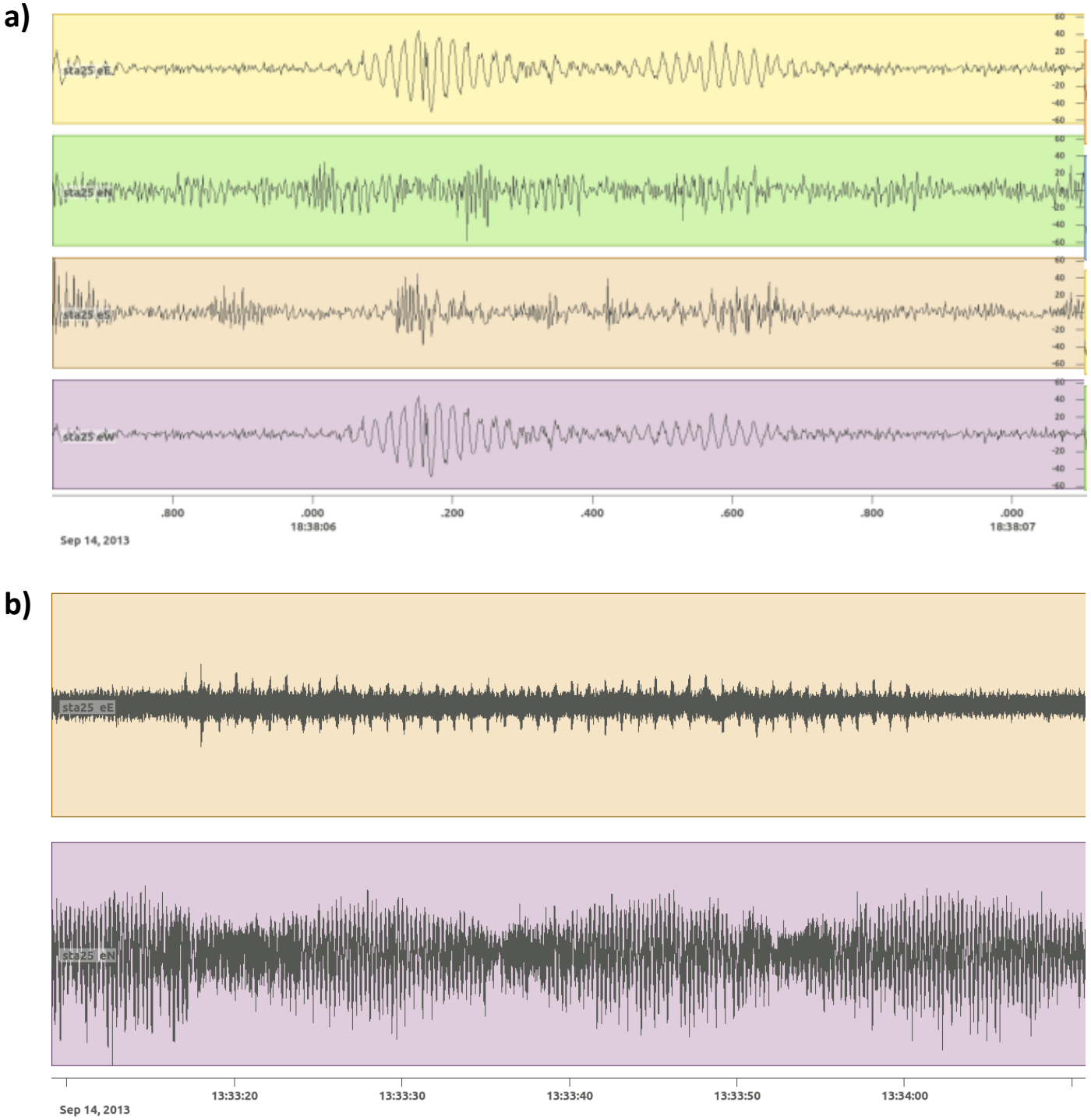

Figure 13: MT e-logger on-site monitoring of Adelaide Airport Aquifer Injection Scheme. Conducted from 13 to 16th September 2013. Testing was conducted in a heavily urbanised setting, within 1 km distance of Adelaide Airport a) a ~1.5 s window time series of filtered data from station 25. Filtering effects applied include a 8 Hz highpass filter, and a 4 Hz width notch filter including harmonics at 50 Hz. The filtering effectively minimised noise, however caused a phase loss for the north and south stations b) A ~60 second unidentified patterned event recorded at station 25. The event was characterised by 1 s pulsations over 45 s, repeating every 2 m. These events were frequently observed across all three stations.

a)

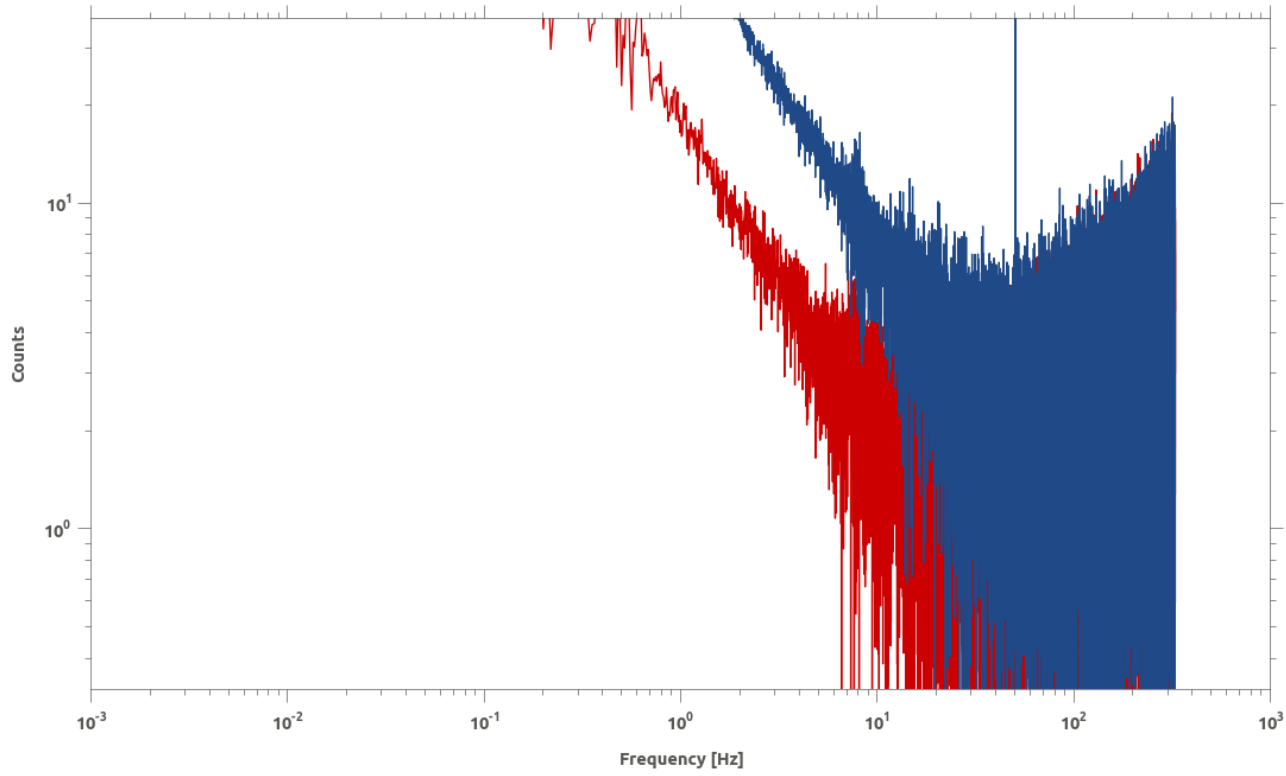

b)

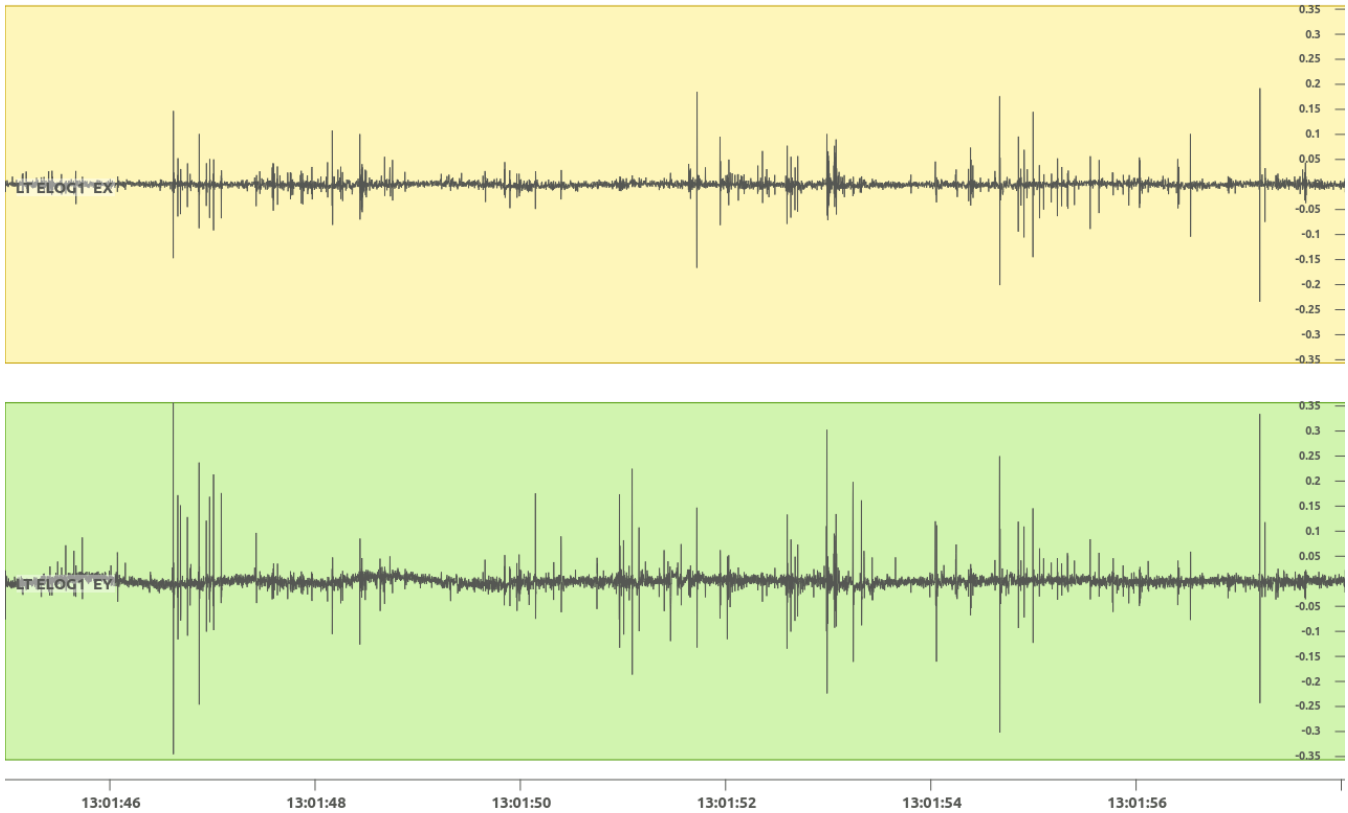

Figure 14: E-logger data collected at Brookfield Conservation Park, Blanchetown, South Australia. a) Amplitude spectrum of a survey with minimal correlated noise. A single outlier peak can be seen at ~50 Hz, however this does not affect data quality. This amplitude spectrum is typical of a successful data acquisition. b) Clean e-logger MT data, separated in Y (east- west) and X (north-east) stations. Minimal correlated sinusoidal noise was recorded, and only uncorrelated events can be seen.

Self Potential Field Logger

SPECIFICATIONS AND CONSTRUCTION OF SP FIELD LOGGER MODEL

A prototype SP field logger was constructed (Figure 15) to monitor for voltage change caused by sub-surface fluid movement on-site of the Adelaide Airport aquifer injection scheme.

A general-purpose data logger *DataTaker DT85 Series 2* recording instrument was used to define and record change in voltages across the 12 electrodes. Its sixteen analogue channels have capacity to record 48 independent simultaneous electrode voltage measurements, meaning ease of expansion to the prototype initial models 12 electrode design. A seismic cable was adapted to host the electrodes. The cable is a total of 120 m in length, hosting an electrode every 10 m with a total of 12 take-out measurement points to host electrodes. Geophone connectors were fitted to passive measurement electrodes that clamp to the take-out measurement points. Electrodes were SDEC France's PMC900, Pb-$PbCl_2$ NaCl unpolarizable electrodes for geophysical measurements. The specialised electrodes are ideally used to measure water flow in soils for use with agronomic science, thus are particularly sensitive to SP signals.

The SP field logger measures voltage between two electrodes separated by some distance. Voltage difference is measured mainly by a function of electric field and self-potential signal. For each electrode position (Electrode 2 (E2) as an example) we measure the following:

$$\Delta V = \left(V_{SP}^{E2} - V_{SP}^{Reference}\right) + E_{induced} * \Delta x \quad (12)$$

Where $E_{induced}$ is the induced electric field, and Δx is the distance between the electrode E2 and the Reference electrode.

Figure 15: Photograph of prototype SP field logger model. The black casing (left) is a watertight hub (approximately 40 cm length) for non-water resistant logger controls. It contains the general purpose datalogger *DataTaker DT8,5* where the logger program is commenced and halted. The datalogger also allows for live inspection of electrode values (in mV) to detect for electrode issues. Batteries are sealed within this box, and a solar panel is used to hold battery charge. Additional batteries can be plugged in externally via water tight connection. The adapted seismic cable (right) has a total length of 120 m, with yellow take-out measurement points for modified geophone connector electrodes (central). The electrode displayed is a SDEC France's PMC900, Pb-$PbCl_2$ NaCl unpolarizable electrode.

SELF POTENTIAL FIELD LOGGER SURVEY:

An overall voltage signal is recorded at each electrode, part of which may include a SP signal generated by natural or engineered sub-surface fluid flow. A survey sample rate of one reading per second was used. The 120 m electrode line was laid in an east to west orientation, with electrodes E1 and E12 furthermost to the east and west respectively.

Monitoring results indicated that all electrodes E1 to E12 followed a generalised large-scale trend (Figure 16). The trend is generated by factors such as shared natural electric field, and

highly correlated unidentified external factors (such as SP signals). Signs of non-natural, external voltage influences are observed through the data. Routine periods of low activity at 0.5, 1.5 and 2.5 days are observed between routine periods of increased voltage difference at 1 and 2 days.

As an electrodes spatial distance to the ground source increases, so too does its potential difference. An electrode can be spatially corrected via calculation of its electric field (mV/m):

$$\frac{Voltage\ (mV)}{Distance\ (m)\ of\ electrode\ to\ ground} = Electric\ Field\ (mV/m) \quad (13)$$

Electrodes can be corrected further of external regional noise by subtracting a single electrode as a reference trace. Using electrode E1 as a reference trace (Figure 17), we can assess the electrodes comparative localised voltage changes.

A generalised trend can still be seen including periods of stable, increased and decreased electric field that is consistent for all electrodes. Strong localised variation changes are notable at time periods of 1, 2 and 2.5 days. The largest variation of electric field is evident in electrodes E12 and E11 within a range of ±1.5 mV/m and 0.5mV/m respectively. All remaining electrodes E10 to E2 have a variation of $\leq$ 0.4mV/m. The unidentified external noise source appears to have an exponential decay of effect, strongest at electrode E12 (furthermost west) and diminishing to have almost no effect by electrode E9 at 30 m distance.

The spatially and regionally noise corrected natural voltage variation and instrument noise envelope was calculated over a 35 minute period, where minimal external voltage activity sources resulted in an electric field of ~0.002mV/m.

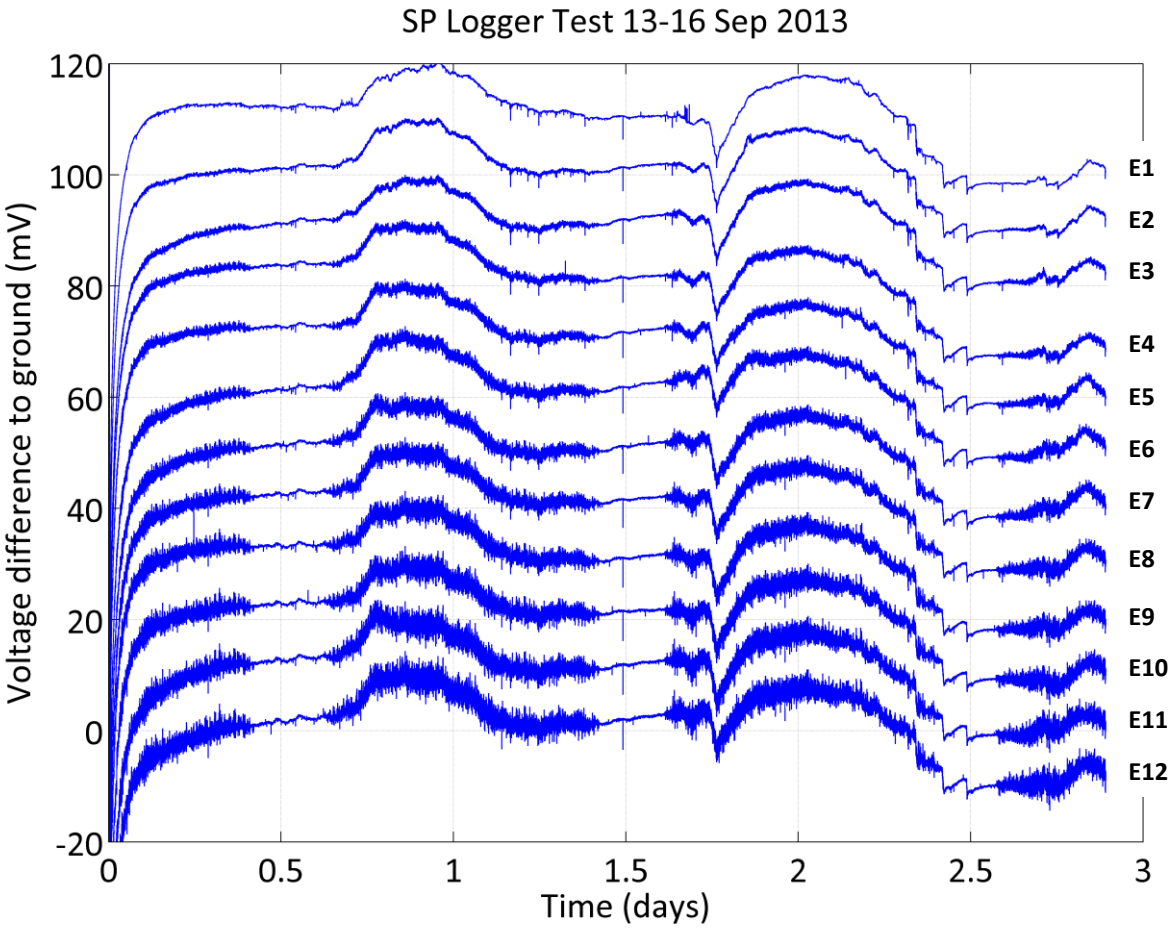

Figure 16: SP Logger's voltage difference to ground (mV). Electrodes E12 to E1 are plotted with a +10 mV increasing difference for comparison and enhanced visualisation of data. Adelaide University Prototype SP Field Logger testing, on-site of Adelaide Airport Aquifer Injection Scheme. Conducted from 13 to 16th September 2013. Testing was conducted during injection and extraction pumping of stormwater fluids to and from sub-surface aquifer at depth of 160 m.

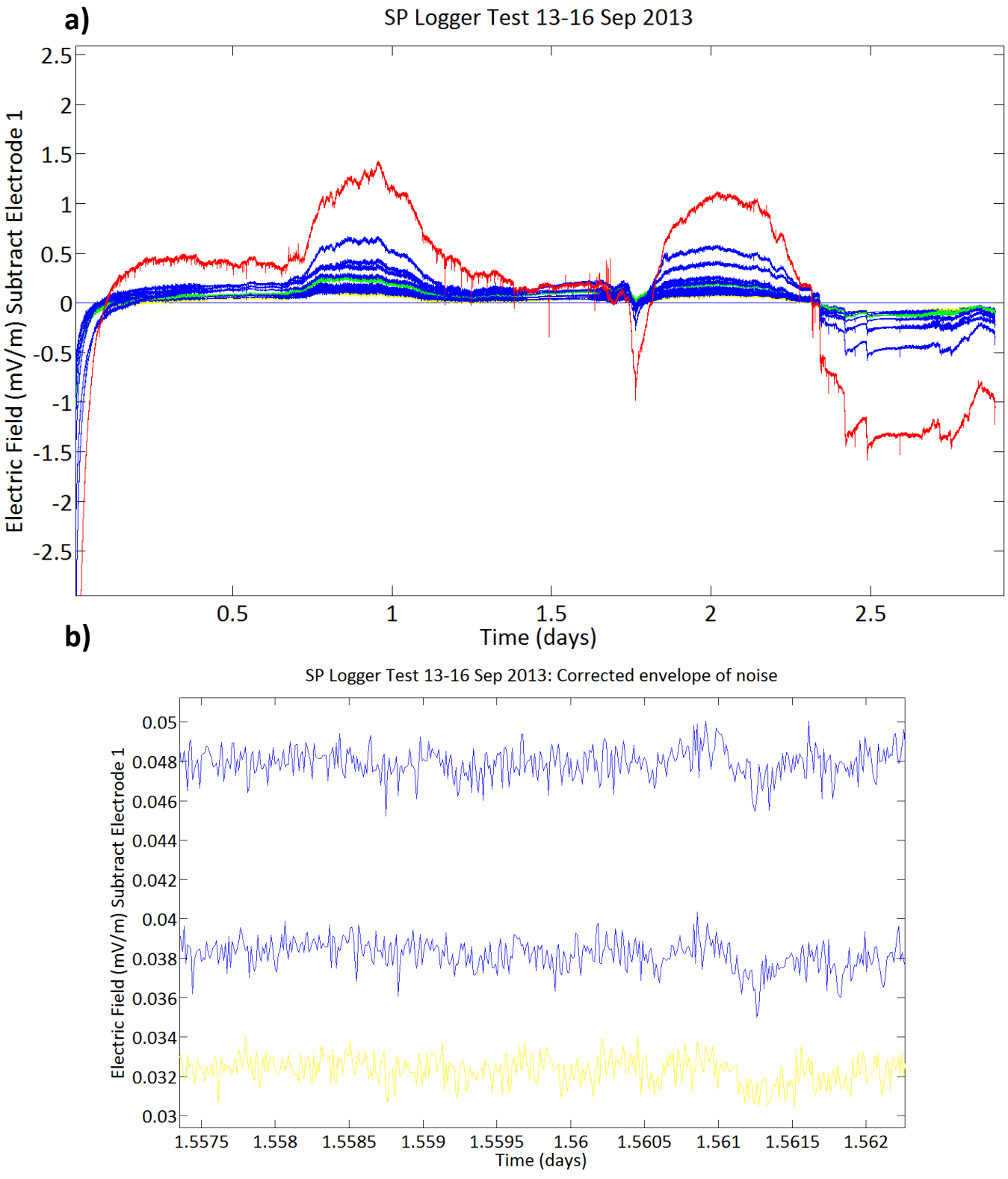

Figure 17: Adelaide University Prototype SP Field Logger testing, on-site of Adelaide Airport Aquifer Injection Scheme. Conducted from 13 to 16th September 2013. Testing was conducted during injection and extraction pumping of stormwater fluids to and from sub-surface aquifer at depth of 160 m. a) SP Logger's electric field (mV/m) subtract Electrode 1. Electrodes are spatially corrected, and E1 is subtracted for use as a stable reference to allow for mapping the variation of electric field amongst all electrodes. Electrode lines are plotted with a +.01mV/m increasing difference for enhanced visualisation of the data. E2 (furthermost east) is yellow, E7 (centralised) is green and E12 (furthermost west) is red to follow order of the electrode line. b) SP Logger's Spatially corrected envelope of natural variation, instrument and unidentified noise sources.

DISCUSSION

Synthetic Data

The use of synthetic data modelling is greatly advantageous for early feasibility research. It is a cost and time effective solution to the dangers of attempting and establishing new endeavours within the industry. However, a synthetic model is based on averaged or assumed values to encapture real life settings, and although practical the accuracy of the model compared against actual data must always be considered within a feasibility study. A synthetic study can only give an insight to probability of failure or success; real world data values may in fact be largely variable or inconsistent to prior understanding. The vast quantity of potential variables possible at an actual Surat Basin CSG site means that while synthetic modelling results indicated the successful potential of monitoring coal seam depressurisation conditions using MT and SP methods, further testing is required before this can be definitively confirmed or denied.

MAGNETOTELLURIC MODELLING

Results confirm that the post- model 2D inversion (Figure 7 b) and pseudosection (Figure 8) have given a relatively accurate representation of the synthetic input data to 550 m depth. An average increase in sub-surface resistivity of approximately 2-4 Ωm between 400 m to 600 m depth was the evidence of change subsequent to CSG depressurisation. However, resistivity values (1000Ω) of the depressurised coal seam were not maintained, and no defined boundaries of the coal seam can be interpreted in results. TE and TM Phase (Figure 8) detected an accurate change in sub-surface structure at approximately 500 m to 550 m depth.

Depressurised coal seam values continue to propogate below 550 m depth and produce inaccurate increased resistivity values. Resistivity increases below approximately 600 m depth were inconsistent to the post-depressurisation input model data. This is likely a result

of inversion smoothing processing (more specifically, the modelling tau value of 50) averaging out the highly resistive coal seam to lower depths.

For future feasibility model studies, as the relative sub-surface depths that are affected by a CSG depressurisation event are known, an area-constrained inversion may contain and clarify coal seam resistivity changes to a higher standard of accuracy and precision. This, in turn, would limit effectiveness to monitor aquifer interaction outside of a coal seam. A balanced decision concerning depth constraint is required, as not to nullify the environmental application of the monitoring technique.

Size and depth of the depressurised coal seam structure was highly accurate, and a constrained inversion will likely improve accuracy of resistivity values. The MT monitoring has shown a great potential of effectiveness for mapping large scale sub-surface change within a CSG project, however further modelling studies and field-testing is required.

SELF-POTENTIAL MODELLING

Based on the SP1 and SP2 synthetic models (Figures10 and 11), conditions for mapping voltage variation will be more difficult during initial stages of depressurisation due to weaker SP signals convoluted with external noise and electrode stability. As the coal seam resistivity increases with time, the SP1 model moves towards a SP2 model and a stronger SP voltage will develop providing a stronger voltage for measure. A stronger voltage gradient will not be as greatly affected by noise and electrode stability.

It must also be noted that in theory a high or increasing SP signal strength does not have a directly correlating relationship with volume of subsurface fluid movement. As the depressurisation event causes a slowly increasing coal seam resistivity, the developing SP

signal strength will increase based on resistivity changes and not changes of fluid volume movement.

Modelling did not take into consideration that the rate of water withdrawal in CSG depressurisation is likely to fluctuate, peaking within early stage pumping. Rate of water removal is dependent upon the geological formation, and rate in which water is removed from a CSG well drastically reduces over time as gas production increases (Australia Pacific LNG 2013). Both models used a standardised pump rate of 20,000ML a day and this value would realistically change on an alternating daily basis, continually changing expected SP signal strength.

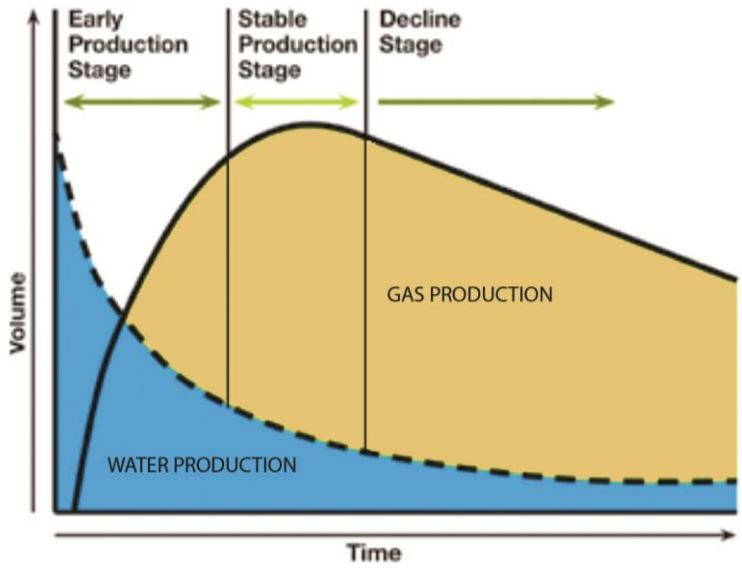

Figure 18: Variation of water and gas production rates within the early production, stable production and decline stages of a CSG well. Subsequently, SP signal strength will be largely affected by fluctuation in fluid extraction. This effect has not been taken into account for models SP1 and SP2, and a steady flow rate has been applied.

The synthetic modelling has given a good understanding of potential SP signal strength caused by the event depressurisation, and indicated how a slowly changing subsurface resistivity will cause a change in signal strength. Values presented in the synthetic models are only assumed averages, and the actual subsurface environment of a coal seam gas project site

will present more obstacles for determining SP signal of a depressurisation event eg. aquifer fluid movement, signal attenuation. However, the model does indicate that a strong and readable SP signal will reach the surface. The results are a positive indicator for developing a next stage on-site SP monitoring feasibility studies.

Equipment Survey

PB-PBCL$_2$ ELECTRODE STABILITY

The MT and SP monitoring electrodes kept in damp ground conditions due to continuous light rainfall through the survey period. If the ground is dry it absorbs the internal solution of the electrode by capillarity, and some salts deposit in places where the solution can evaporate both external to and within the electrode. The electric resistance strongly increases during this dehydration (Petiau 2000).

For future feasibility monitoring over greater lengths of time (weeks to months) in dry ground conditions, steps must be taken to assure electrode stability for accurate measurement. Over one year, the measurement error, defined as the standard deviation of the difference between the measured potential and the true SP at a given time, is estimated to be 5 mV (Perrier and Pant 2005). Mitigation of the dehydration process involves grounding electrodes at a depth great enough (greatly dependent on localised site conditions) to discourage electrode evaporation and absorption of the air humidity, and use of a salted clay mud in order to guarantee a good contact of the electrode with the ground (Petiau 2000).

MAGNETOTELLURIC E-LOGGER

On-site data collected was consistent through all three e-loggers (Figure 12 a). The partially noise affected east and west stations showed clearly correlated events. Filtering could only provide further clarity to east and west stations. However, the north and south stations were

too greatly affected by noise, and therefore could not show consistent and clear events patterns.

Sinusoidal noise at the 50 Hz frequency range is an affect commonly attributed to localised power lines and communications devices in urbanised settings (Fontes et al. 1988).It is also likely that noise at 4 Hz frequency, and the reoccurring patterned events in east and west channels (Figure 13 b) were causes of anthropogenic influence.

It is unlikely that rural based CSG projects will have anthropogenic noise sources comparable to a near city Adelaide Airport testing site. Machinery, cellular phone devices and pump stations on-site of a CSG project will produce negligible noise that can be filtered using processes discussed.

The e-logger model has been field tested previous to this survey (Figure 15), where it successfully produced a clean data set with no correlated noise, and only uncorrelated data values with distinct events.

Although testing data collected was heavily affected by sinusoidal noise, we can deduce that the disrupted north and south signal consistent in all loggers is not a result of the models design. Subsequently, we can conclude that the e-logger model can effectively monitor MT signals in further feasibility studies on-site of a CSG project.

SELF POTENTIAL FIELD LOGGER

The voltage readings of all electrodes were affected by periodic external influences throughout the full length of survey (Figure 15). The external influence is most likely a result of anthropogenic factors due to the consistent and periodic nature of the null voltage activity events transitioning to increasing voltage activity events. Pump operation contractors confirmed that bore pump stations were actively injecting and extracting sub-surface fluids for reuse and irrigation needs over the length of survey period. However, a schedule of pump operating times could not be obtained for correlating the periodic events.

Spatially and noise corrected electrodes displayed strong evidence of localised electric field changes (Figure 17). The external influence caused the highest localised variation to electrode E12 (westernmost electrode) which diminished towards electrode E2 (easternmost electrode). Based on locality of injection and extraction bores due south-west of the survey, changes in electrodes localised electric field results support the theory that the source of external influence was in fact SP signal generated by engineered sub-surface fluid movement (Figure 17). However, the external signal appears to be exponentially decaying from west to east; synthetic modelling suggests that SP signal should in fact show a linear decay from the source. If the external noise source is in fact a SP signal, then there is a potential secondary noise source with a more localised voltage signal also affecting only electrodes E12-E10 that is causing an appeared exponential decay.

Although spatial and survey external noise can be corrected for all survey electrodes to compare localised change (Figure17), there is still the potential for unwanted and very localised effects (such as soil chemical interaction) on a individual or reference electrode (E1) that would disrupt correction. Revil et al (2012) describes the use of a static reference electrode in a bentonite clay covered hole. The presence of the bentonite mud will reduce

local effects and modifies the electrical potential at the contact between the electrode and the ground. Therefore, the potential of this station is arbitrary making the reference stable, but it does not reduce the potential to zero.

The averaged corrected electric variation and instrument noise envelope of the SP logger was observed over very low signal activity (Figure 17 b) to be approximately ±0.002mV/m. Electrodes in a survey line therefore must record a variance of SP signal higher than the noise envelope to generate an effective reading of localised subsurface conditions between .

We can apply results collected from the synthetic SP1 and SP2 models to the following simple formula and calculate the linear gradient of SP signals:

$$\frac{SPmax_{mV}}{5000m} \times 10m \tag{13}$$

Where Max_{mV} is the highest SP value found at the surface, 5000m is the total radius of SP signal noise caused by the depressurisation event, and 10m is the standard length between survey electrodes:

$$SP1\text{: } \frac{12.9mV}{5000m} \times 10m = 0.0258mV/m \ < 0.002mV/m\ corrected\ noise \tag{14 a}$$

$$SP2\text{: } \frac{129mV}{5000m} \times 10m = 0.258mV/m \ < 0.002mV/m\ corrected\ noise \tag{14 b}$$

This concludes that the proposed gradient of voltage change per 10 m in model SP1 (0.0258mV) and SP2 (0.258mV/m) is higher than the noise envelope and localised signal between neighbouring electrodes can be mapped by the field logger constructed. However, localised noise levels within a CSG project area may be higher due to additional influences such as natural groundwater movement external of the coal seam (Todd and Mays 1980).

The natural variation and instrument noise envelope can be processed using various techniques such as box filters to give a further reduced noise envelope. Effectiveness of

processing techniques on raw survey data was considered outside thesis scope, as we were motivated to primarily assess the effectiveness of the instrumentation alone.

On-site SP monitoring and feasibility research presents strong evidence that localised SP signal gradients caused by depressurisation pumping can be readily detected and mapped. further on-site CSG feasibility studies must be conducted for this statements to be realistically conclusive.

Overall, The SP field logger survey produced promising results, highlighting the design and construction of the instrument was effective for the required job. The prototype has provided good feedback for the construction of a next stage SP field logger. The set-up and operation of the instrument was completed in a timely and hassle free manner, two underestimated features of successful field equipment. Criticisms to the design include: the high weight of the seismic cables making transportation difficult; and the inability to analyse survey data off-site and in real time to assure quality control.

CONCLUSIONS

Magnetotelluric synthetic modelling was shown to effectively map changes in subsurface structure caused by a coal seam depressurisation event; further work using confined modelling is required to map a more accurate resistivity change. The modelling provided evidence that in our proposed Surat Basin CSG sub-surface conditions, the monitoring will detect a measurable change.

The MT e-logger field test data acquired anthropogenic sinusoidal noise issues, particularly affecting the north and south channels of all loggers. Previous to this, the logger has successfully collected surface MT data free of correlated noise; thus, we can be confident that this was not a fault of the loggers design or construction.

Synthetic SP modelling provides substantial evidence suggesting that in a CSG depressurisation, SP monitoring can successfully map localised fluid flow at the surface. The SP signal's strength and gradient are significantly high enough for mapping localised electrode change amongst correlated noise affects; in particularly, the strength of SP signal during mid and late stage depressurisation when coal seam resistivity has increased by a factor of 10.

The prototype SP logger has provided effective feedback for the construction of an improved, more functional field SP logger model. The instrument design effectively logged varying localised voltage values with high precision, and an unaffecting instrument noise envelope. A strong undefined varying voltage signal correlated spatially to the Adelaide Airport Aquifer Injection Scheme pump location, believed to be a pump induced SP signal.

SDEC France's PMC900, Pb-$PbCl_2$ NaCl unpolarizable electrodes measured precise voltage values across all electrodes. The PMC900 style of Pb-$PbCl_2$ electrodes are considered as a most stable, minimal drift electrode choice for long term monitoring conditions.

Combining use of MT and SP techniques can give monitoring coverage of both large scale and localised subsurface fluid migration. Monitoring equipment has been tested for precision and reliability, and surveys can be established in a relatively short time frame. Surveys are inexpensive in comparison to alternative monitoring techniques, and have minimal to no ongoing running and maintenance costs. Based on synthetic modelling and field equipment testing, results concluded that MT and SP geophysical monitoring of a CSG depressurisation setting is a viable technique that may demonstrate to be a value-adding tool, or a formidable opponent of current industry monitoring techniques.

Monitoring equipment tested can be established in a relatively short time frame, has minimal to no ongoing running costs. If the technique proves to be successful, it is pioneering a new CSG industry standard of resource and environmental monitoring.

This thesis has presented a feasibility study for use of magnetotelluric and self-potential geophysical methods for the monitoring of a coal seam depressurisation event. Whilst it has drawn mainly promising outcomes, further research and testing is necessary to draw on an outcome conclusion of monitoring success.

ACKNOWLEDGEMENTS

I would like to thank my primary supervisor Professor Graham Heinson for his guidance and feedback throughout this project. I would also like to thank Dr. Stephan Thiel, Dr. Lars Kreiger, and Dr Mike Hatch for their suggestions, input and guidance. Special thanks to A. Jardani for his SP2DINV inversion model input, SA Water for testing site access, and Nigel Cook for fieldwork help. Also, a warm thanks to Goran Boren for teaching and guiding the construction of a prototype SP field-logger. Without the help of any of these people, the completion of my final thesis would not have been possible.

REFERENCES

AUSTRALIA PACIFIC LNG 2013 Fact sheet: Coal seam gas production and groundwater supplies.

AUSTRALIAN GOVERNMENT NATIONAL MESUREMENT INSTITUTE 2013 Environmental Testing-Coal Seam Gas.

BEAR J. 1979 Hydraulics of Groundwater. McGraw-Hill Book Company, New York.

BIRCH F. S. 1993 Testing Fournier's Method for Finding Water Table from Self-Potential, *Ground Water,* vol. 31, no. 1, pp. 50-56.

COMPAGNIE GÉNÉRALE DE GÉOPHYSIQUE S. A. 2013 Microseismic: Applications.

COX R. 2013 Impact of CSG on Groundwater in Qld. Queensland Government, Department of Natural Resources and Mines: Office of Groundwater Impact Assessment.

DOMENICO P. & SCHWARTZ W. 1998 Physical and chemical hydrogeology. (2nd edn edition). Wiley and Sons, Inc, New York.

DRISCOLL F. 1986 Groundwater and wells. (2nd edn edition). Johnson Filtration Systems, Inc., St. Paul, Minnesota.

EXON N. F. 1976 Geology of the Surat Basin in Queensland. Bulletin. Australian Government, Geoscience Australia.: Bureau of Mineral Resources, Geology and Geophysics, Canberra.

FAGERLUND F. & HEINSON G. 2003 Detecting subsurface groundwater flow in fractured rock using self-potential (SP) methods, *Environmental Geology,* vol. 43, no. 7, pp. 782-794.

FETTER C. 1994 Fetter CW (1994) Applied hydrogeology, 3rd edn. Prentice-Hall, Englewood Cliffs.

FETTER C. 1999 Contaminant hydrogeology. Prentice Hall, Upper Saddle River, New Jersey.

FITTERMAN D. V. 1978 Electrokinetic and magnetic anomalies associated with dilatant regions in a layered Earth, *Journal of Geophysical Research: Solid Earth,* vol. 83, no. B12, pp. 5923-5928.

FONTES S. L.*, et al.* 1988 Processing of noisy magnetotelluric data using digital filters and additional data selection criteria, *Physics of the Earth and Planetary Interiors,* vol. 52, no. 1–2, pp. 30-40.

HEISE W.*, et al.* 2008 Three-dimensional modelling of magnetotelluric data from the Rotokawa geothermal field, Taupo Volcanic Zone, New Zealand, *Geophysical Journal International,* vol. 173, no. 2, pp. 740-750.

HELM D. C. 1987 Three-dimensional consolidation theory in terms of the velocity of solids. Géotechnique. pp. 369-392.

HÖRDT*, et al.* 2000 A first attempt at monitoring underground gas storage by means of time-lapse multichannel transient electromagnetics, *Geophysical Prospecting,* vol. 48, no. 3, pp. 489-509.

ISHIDO T. & MIZUTANI H. 1981 Experimental and theoretical basis of electrokinetic phenomena in rock-water systems and its applications to geophysics, *Journal of Geophysical Research: Solid Earth,* vol. 86, no. B3, pp. 1763-1775.

ISHIDO T. & PRITCHETT J. W. 1999 Numerical simulation of electrokinetic potentials associated with subsurface fluid flow, *Journal of Geophysical Research: Solid Earth,* vol. 104, no. B7, pp. 15247-15259.

JOUNIAUX L.*, et al.* 2009 Review of self-potential methods in hydrogeophysics, *Comptes Rendus Geoscience,* vol. 341, no. 10–11, pp. 928-936.

KAUFMAN A. A. & KELLER G. V. 1981 The magnetotelluric sounding method. Elsevier, Amsterdam.

KLOHN CRIPPEN BERGER LTD 2012 Forecasting CSG water production in the Surat & southern Bowen basins. Prepared for Department of Natural Resources and Mines, Queensland Government.

KNIGHT R.*, et al.* 2010 Geophysics at the interface: Response of geophysical properties to solid-fluid, fluid-fluid, and solid-solid interfaces, *Reviews of Geophysics,* vol. 48, no. 4, p. RG4002.

MALAMA B., KUHLMAN K. L. & REVIL A. 2009 Theory of transient streaming potentials associated with axial-symmetric flow in unconfined aquifers, *Geophysical Journal International,* vol. 179, no. 2, pp. 990-1003.

MALAMA B., REVIL A. & KUHLMAN K. L. 2008 A semi-analytical solution for transient streaming potentials associated with confined aquifer pumping tests, *Geophys J,* vol. 176, no. 3, pp. 1007-1016.

NGHIEM L. D.*, et al.* 2011 Treatment of coal seam gas produced water for beneficial use in Australia: A review of best practices, *Desalination and Water Treatment,* vol. 32, no. 1-3, pp. 316-323.

OVERBEEK J. 1952 IV. Electrochemistry of the double layer and V. Electrokinetic phenomena., *Colloid Science,* vol. vol I, no. irreversible systems, pp. pp 115-243.

PEACOCK J. R.*, et al.* 2012 Magnetotelluric monitoring of a fluid injection: Example from an enhanced geothermal system, *Geophysical Research Letters,* vol. 39, no. 18, p. L18403.

PERRIER F. & PANT S. R. 2005 Noise Reduction in Long-term Self-potential Monitoring with Travelling Electrode Referencing, *pure and applied geophysics,* vol. 162, no. 1, pp. 165-179.

PETIAU G. 2000 Second Generation of Lead-lead Chloride Electrodes for Geophysical Applications, *pure and applied geophysics,* vol. 157, no. 3, pp. 357-382.

REVIL A. & FLORSCH N. 2010 Determination of permeability from spectral induced polarization in granular media, *Geophysical Journal International,* vol. 181, no. 3, pp. 1480-1498.

REVIL A.*, et al.* 2012 Review: Some low-frequency electrical methods for subsurface characterization and monitoring in hydrogeology, *Hydrogeology Journal,* vol. 20, no. 4, pp. 617-658.

REVIL A., PEZARD P. A. & GLOVER P. W. J. 1999 Streaming potential in porous media: 1. Theory of the zeta potential, *Journal of Geophysical Research: Solid Earth,* vol. 104, no. B9, pp. 20021-20031.

RIZZO E.*, et al.* 2004 Self-potential signals associated with pumping tests experiments, *Journal of Geophysical Research: Solid Earth,* vol. 109, no. B10, p. B10203.

SILL W. R. 1983 Self-potential modeling from primary flows, *Geophysics,* vol. 48, no. 1, pp. 76-86.

SIMPSON F. & BAHR K. 2005 Practical Magnetotellurics. Cambridge University Press.

SOUEID AHMED A.*, et al.* 2013 SP2DINV: A 2D forward and inverse code for streaming potential problems, *Computers & Geosciences,* vol. 59, no. 0, pp. 9-16.

SPICHAK V. & MANZELLA A. 2009 Electromagnetic sounding of geothermal zones, *Journal of Applied Geophysics,* vol. 68, no. 4, pp. 459-478.

STREICH R., BECKEN M. & RITTER O. 2010 Imaging of CO2 storage sites, geothermal reservoirs, and gas shales using controlled-source magnetotellurics: Modeling studies, *Chemie der Erde - Geochemistry,* vol. 70, Supplement 3, no. 0, pp. 63-75.

TAULIS M. & MILKE M. 2013 Chemical variability of groundwater samples collected from a coal seam gas exploration well, Maramarua, New Zealand, *Water Research,* vol. 47, no. 3, pp. 1021-1034.

TODD D. K. & MAYS L. W. 1980 Groundwater Hydrology Edition.